Smart Antenna RF Front-end For WLAN and SDARS

by

Yu Bai

A thesis
presented to the University of Waterloo
in fulfillment of the
thesis requirement for the degree of
Master of Applied Science
in
Electrical and Computer Engineering

Waterloo, Ontario, Canada, 2006

Author's Declaration

I hereby declare that I am the sole author of this thesis. This is a true copy of the thesis, including any required final revisions, as accepted by my examiners.

I understand that my thesis may be made electronically available to the public.

Abstract

This thesis presents RF front-end system design for both WLAN (Wireless Local Area Network) and SDARS (Satellite Digital Audio Radio System) applications using adaptive smart antenna technique. It is important to understand that smart antenna system with adaptive beam-forming provides the following advantages:

1. It can concentrate radio transmission on specific directions by modifying transmit/receive phase and amplitude characteristics, and therefore provides greater coverage and increased capacity.

2. It can greatly reduce multi-path fading effect and co-channel interference.

This thesis first presents a complete 4-element smart antenna system for IEEE 802.11b/g WLAN applications. The prototype presented can interconnect with an of-the-shelf WLAN network card. The system is controlled via a microcontroller that adjusts the array pattern to capture the best signal. Measurements show that the system can increase the RSSI (Received Signal Strength Indicator) level significantly and therefore the SNR (Signal to Noise Ratio). This prototype is the first step towards a novel DBF (Digital Beam-Forming) smart antenna architecture.

The second part of the thesis presents a 2-element smart antenna system for SDARS application. This prototype can be connected with an of-the-shelf SDARS digital receiver. The system was tested in a chamber and measurements show a controlled beam and increased gain. Ansoft HFSS was used to simulate the 2-element smart antenna and validate the testing results.

Acknowledgements

I would like to express my deep thanks to my supervisor, Dr. Safieddin Safavi-Naeini. Without his continues guidance and support, I could not finish this thesis. I would also like to thank my readers, Dr. Omar Ramahi and Dr. Hamed Majedi, for their comments and careful reading of the draft.

I would like to thank Cutberto Santillan and Mircea Hossu for providing me countless helps. I am so lucky to have you guys as my friends.

Thanks my parents for their love and continues encouragement. Although they were not in Waterloo when I was writing the thesis, I can always feel their support.

Last, I owe great thanks to my life partner, Joanna Zhou, for her love, encouragement, and being my company for countless good or bad days.

Table of Contents

List of Tables

List of Figures

Chapter 1
Introduction

Wireless communication has come a long way since the prediction of existence of electromagnetic waves by Maxwell in 1867, and the invention of the wireless concept by Marconi in 1897. In the past few decades, wireless communication applications such as cell phone, WLAN (wireless local area network), SDARS (satellite digital audio radio service), satellite TV and cordless phone etc. have come into every part of our life. Especially in the recent years, personal wireless communication is getting more and more popular and is continuing to grow at an exponential rate. This growth has triggered a tremendous demand for not only higher transmission capacity, but also greater coverage area and better quality of service [1].

The availability of basic resources is one of the fundamental limitations of any business. It is true for wireless communication too. After years of having more bandwidth available than needed, we soon find ourselves facing a potential shortfall in capacity. The new bandwidth-hungry Internet, multimedia and video streaming are coming. Therefore, new technologies are needed to be developed to accommodate this increasing demand and to make use of our limited resources.

Smart antenna with adaptive beam-forming has emerged as a key technology to solve this problem, and holds a lot of promises for the future of wireless communication. This is why throughout the world, including Canada, there is significant research and development on smart antenna for wireless system right now.

Though smart antenna techniques are new in the area of wireless communication, the technology itself was introduced back in 1960's. Early smart antenna technology was deployed in military communication systems, where narrow beams were used in order to avoid interference arising from noise and other jamming signals [1]. Until recently, the use of smart antennas had been limited to military applications. But performance gains in cost-effective RFIC (Radio Frequency Integrated Circuit), digital signal processing, and improved algorithms have extended the smart antenna concept into commercial wireless communication industry.

1.1 A Simple Analogy for Adaptive Smart Antennas

An intuitive analogy for adaptive antenna system is to close our eyes and move around a music source. It will be interesting to notice that we can still locate the music source without seeing it. This is because we hear the sound wave through our two ears and the wave arrives at each ear at a different time. Our brain, which is like a specialized signal processor, does a large amount of calculations to correlate information and compute the location of the source. Our brain also adds the strengths of the signals from each ear together so that we can perceive the sound in one chosen direction as being almost twice as loud. Further more, when there are multiple music sources, our brain also tune out unneeded interference and focus on one specific source at a time.

An adaptive smart antenna system does the similar thing, by using antennas instead of ears. It can consist of more than two antennas, and it can both listen (receive) and talk (transmit). It also has the similar ability to differentiate between desired and undesired signals.

1.2 Omni-directional Antennas

Antennas are electromagnetic devices that convert electrical signals containing energy and information to EM (electromagnetic) waves and vice versa.

Since the early days, there has been the simple dipole antenna, which radiates and receives equally well in all directions. To transmit signals to a terminal user, this dipole antenna broadcasts omni-directionally outward. A short dipole is a very poor radiator. However when the length approaches half-wavelength the dipole becomes an efficient and popular antenna commonly referred to as half-wave dipole antenna as shown in Figure 1.1.

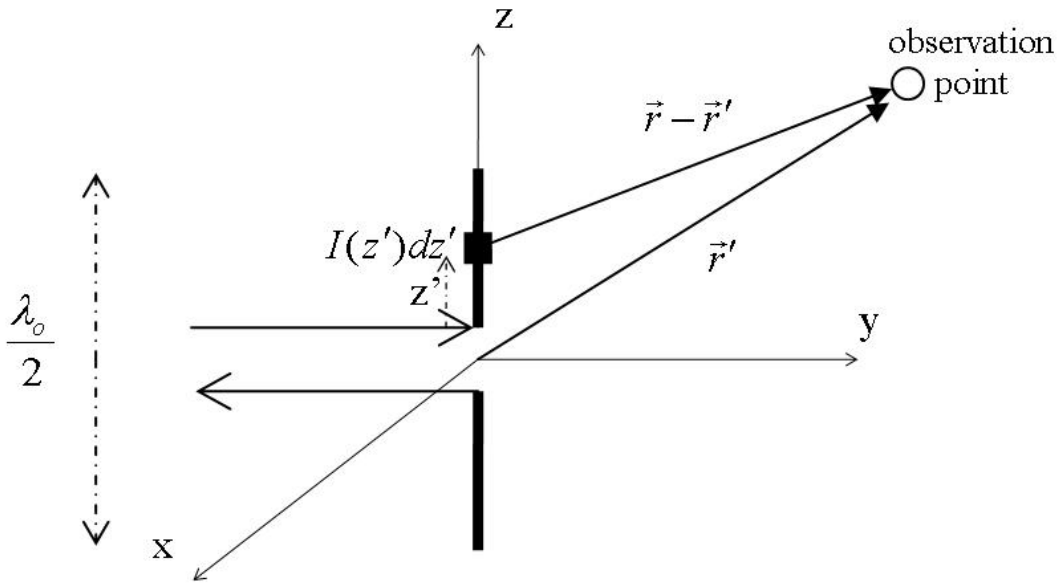

Figure 1.1: Half-wave Dipole

Close to resonance frequency the current distribution over the half-wavelength dipole is nearly sinusoidal.

$$I(z') = I_o \cos(z'), \quad |z'| \le \frac{\lambda_o}{2} \tag{1.1}$$

The far (radiated) field approximation is found using the following equations [2]:

$$A_Z(\vec{r}) \approx \frac{\mu_o e^{-jk_0 r}}{4\pi r} \int_{-\lambda_0/2}^{+\lambda_0/2} I(z') e^{jk_0 z' \cos\theta} dz' = \frac{\mu_0 I_0 e^{-jk_0 r}}{2\pi k_0 r} \left[\frac{\cos\left(\frac{\pi}{2}\cos\theta\right)}{\sin^2\theta} \right] \tag{1.2}$$

$$E_\theta = j\omega A_Z(\vec{r}) \sin\theta = \frac{jZ_0 I_0 e^{-jk_0 r}}{2\pi r} \left[\frac{\cos\left(\pi/2 \cos\theta\right)}{\sin\theta} \right] \tag{1.3}$$

$$H_\varphi = E_\theta / Z_0 \tag{1.4}$$

By using the formulas 1.2 and 1.3, the radiation pattern of an omni-directional antenna is shown below in Figure 1.2.

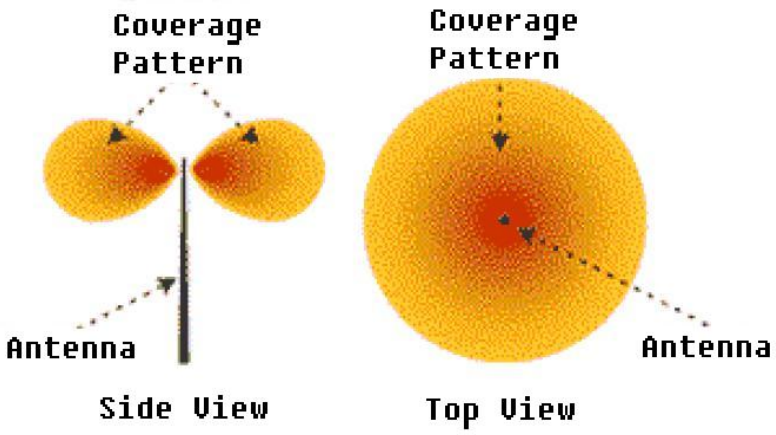

Figure 1.2: Radiation Pattern of Half-wave Dipole [3]

Since it broadcasts omni-directionally, this unfocused pattern scatters signals while reaching desired users with only a small percentage of the overall radiation energy, often too weak. Given this limitation, we can not overcome the problem by simply boosting the broadcast signals because it will introduce interference to adjacent channels.

1.3 Directional Antennas

In order to increase the efficiency and directivity of the omni-directional antennas, the radiating current should be distributed over a larger area. There are other types of antennas to make the radiation beam narrower, such as aperture antennas. Take a conventional cellular base tower for example; we can split 360° area into three 120° subdivisions with each directional antenna covering one subdivision. Figure 1.3 below shows the radiation pattern of a directional antenna.

While directional antennas radiate more efficiently in a prescribed direction by using a much narrower beam which allows reuse of channels, they do not overcome the major disadvantages of omni-directional antennas such as co-channel interference [3].

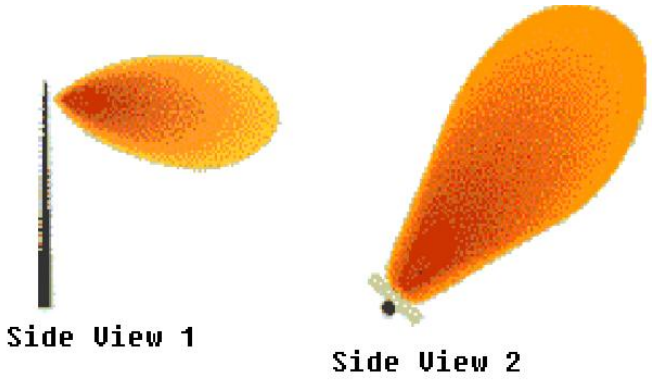

Figure 1.3: Radiation Pattern of Directional Antennas [3]

1.4 Smart Antenna System

Smart antenna system can maximize SNR (Signal to Noise Ratio) adaptively in a time-varying environment. Therefore it can increase the performance characteristics of a mobile terminal in a wireless communication terminal. In the following section, different types of smart antenna systems are described.

1.4.1 Multibeam Smart Antenna System

A multibeam antenna system, which is the simplest form of smart antenna system, consists of a number of fixed beams with one beam turned on towards the desired signal as illustrated in Figure 1.4.

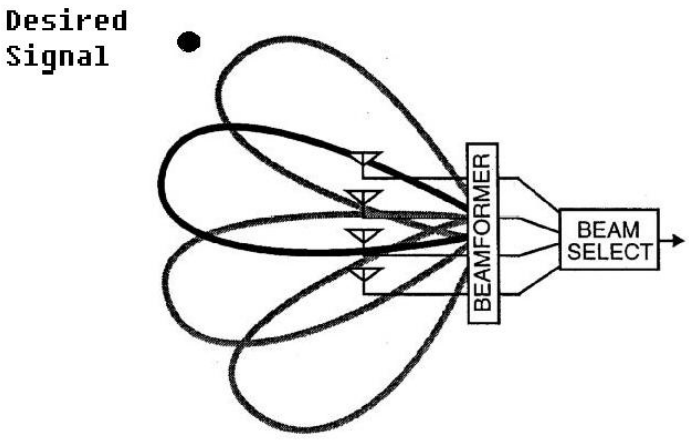

Figure 1.4: Multibeam Smart Antenna System [4]

This antenna system detects signal strength and chooses the best signal from several predetermined fixed beams, and it can switch from one beam to another as the location of the desired signal changes. The problem with multibeam smart antenna is that a maximum signal can not always be reached due to the finite number of stationary beams.

1.4.2 Adaptive Array Smart Antenna System

Adaptive phased array smart antenna system can effectively locate and track signals to dynamically minimize interference and maximize intended signal reception. It consists of multiple antenna elements whose phases can be controlled. Then the receiving signals are weighted and combined. Figure 1.5 shows the components block diagram of a planar phased array smart antenna system. Derivations of antenna radiation and gain will follow after the block diagram.

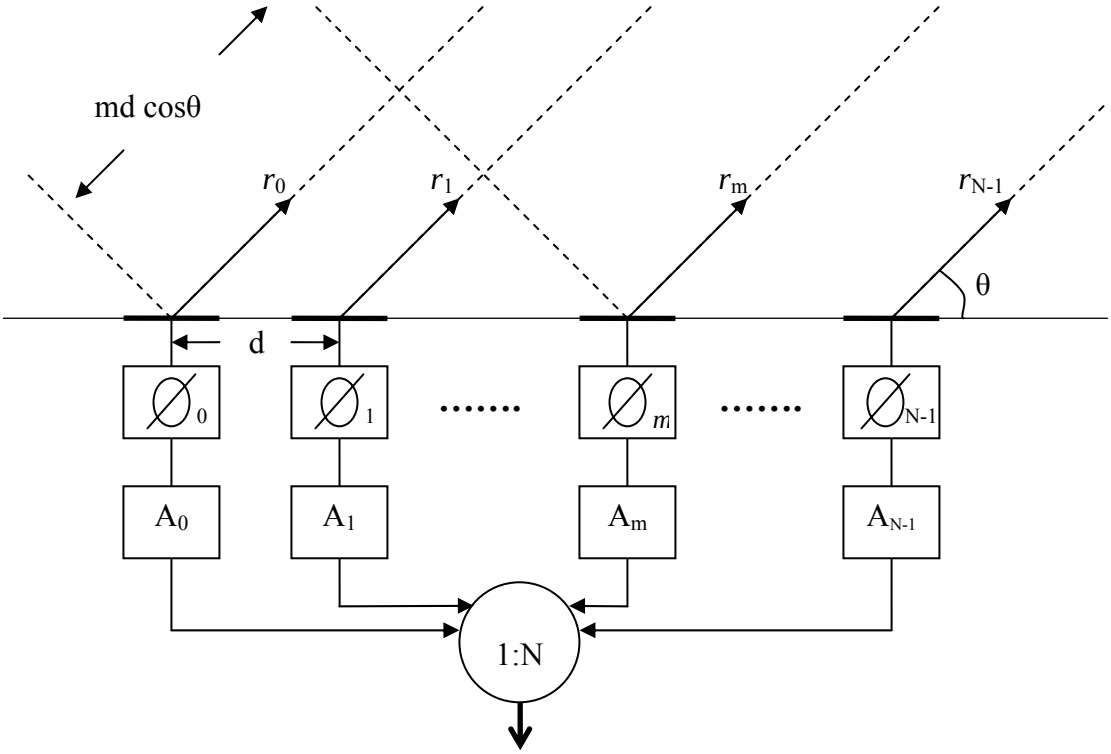

Figure 1.5: Phased Array Smart Antenna Block Diagram

Each antenna element excitation is controlled by amplifier A_m and phase shifter ϕ_m. Therefore the complex excitation coefficient of the m^{th} element can be defined as:

$$I_m = A_m e^{j\phi_m} \tag{1.5}$$

By observation from a faraway point, the radiation generated by each antenna element is the same except for phase. For the purpose of simplicity, let's assume the array is uniformly spaced array, and the inter-element spacing is d. By taking the left most element as our reference, the distance difference to the observation point of the m^{th} antenna is given by [2]:

$$r_m \approx r_0 - md\cos\theta \tag{1.6}$$

The E field of antenna array at the far field observation point is the combination of E fields due to each antenna element, and is given as

$$\vec{E}(r,\theta,\varphi) = \vec{E}_e(r,\theta,\varphi)\left|\sum_{m=0}^{N-1} I_m e^{+jmkd\cos\theta}\right| \tag{1.6}$$

$$\vec{E}_e(r,\theta,\varphi) = \vec{f}_e(\theta,\varphi)e^{-jkr_0}/r_0 \tag{1.7}$$

Array factor can be defined as

$$AF(\theta,\varphi) = \sum_{m=0}^{N-1} I_m e^{+jmkd\cos\theta} \tag{1.8}$$

Therefore by adjusting the phase shifter of each antenna element, we can achieve the goal of maximizing the gain of the antenna array. By changing the amplitude and phase of the antenna element excitation, the radiation pattern of the array can be reshaped in real time. This essentially always puts a main beam in the direction of the desired signal and nulls in the direction of the interferences as it is illustrated in Figure 1.6.

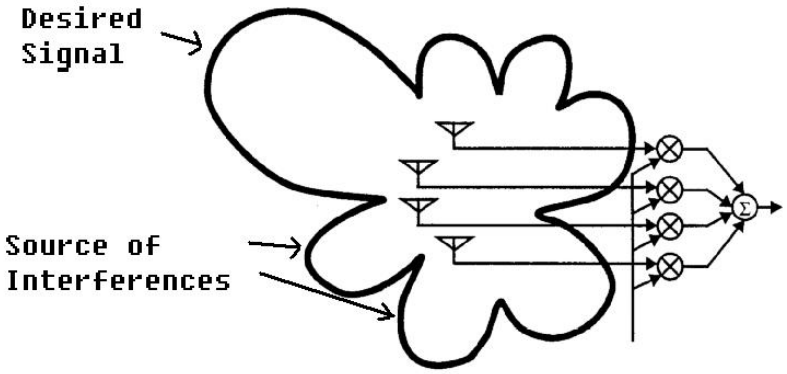

Figure 1.6: Adaptive Phased Array Smart Antenna System [4]

1.4.3 Diversity Antenna System

Diversity antenna system is a special case of an adaptive array system. The operation principle is described below.

A source antenna radiates RF energy in more than one definite direction. Multipath is the scenario where transmitted signal is reflected by physical structures, creating multiple signal paths between the transmitter and the receiver. Figure 1.7 illustrates a multipath situation.

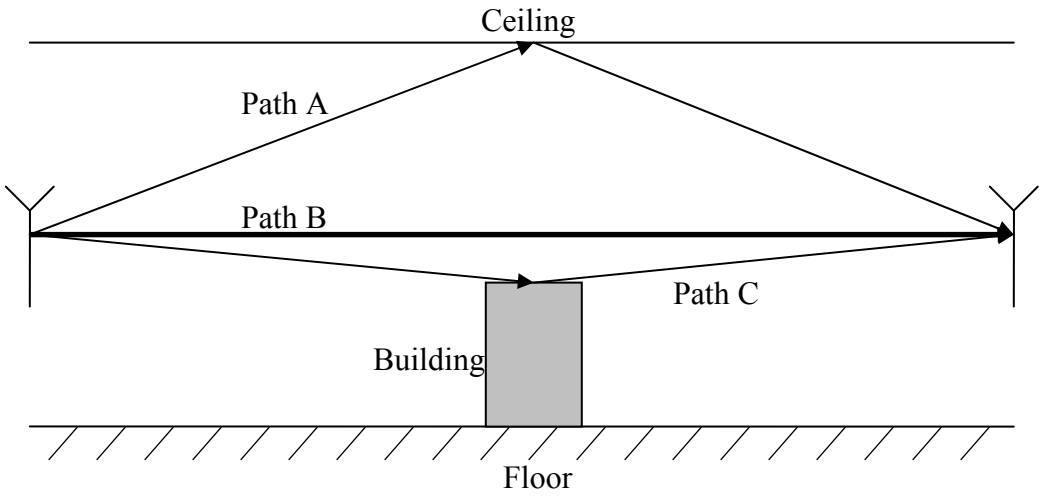

Figure 1.7: A Multipath Scenario

As we can see from the above figure, waves travel farther and arrive later through path A. The longer distance will introduce phase shift. When multipath waves are out of phase, reduction in signal strength and decrease of SNR will occur, which is called multipath fading.

Multipath fading issue can be eased by diversity antenna system. Diversity antenna system is a kind of smart antenna system where the antennas are differently located at optimal positions, either planar or conformal. Simplest diversity reception scheme uses a simple selection algorithm which chooses the antenna with the maximum output signal. Assuming that at least one antenna will be in a favorable location at a given time, this system continually switches between antennas in order to achieve the best SNR.

1.5 Organization of Thesis

This first chapter has already provided an introduction and background study on smart antenna and diversity antenna system. Chapter two introduces an interesting smart antenna and radio front-end architecture for WLAN application. It will describe and evaluate a WLAN smart antenna prototype constructed from regular of-the-shelf components. Testing results are provided and analyzed. Chapter three introduces smart antenna technique and diversity technique to another application, namely SDARS. Simulation using Ansoft HFSS will be demonstrated. Finally testing results will be provided. They will also be analyzed and compared with simulation results.

Chapter 2
Smart Antenna and Radio Front-end for WLAN Application

2.1 Introduction

WLAN has become more and more popular in the recent years with high-speed data rate required to comply with the requirements of advanced wireless communication services such as new bandwidth-hungry Internet, multimedia, and video streaming. Soon we find ourselves facing a potential shortfall in capacity. The proliferation of WLAN base stations and increasing user density combined with demands for higher data rates at higher frequencies has significantly increased the importance of multipath fading and co-channel interference issues. Increasing the range of WLAN systems and reducing the dead spot areas within buildings is also a priority [5]. Therefore, interests in new technologies research have been generated to improve performance and re-use of our limited resources.

Smart antennas have emerged to address all these issues and therefore dramatically improve system performance. Smart antenna system with adaptive beam forming capability has proven to be very effective in suppression of co-channel interference and combating of multipath fading issues [6].

2.2 Proposed System Architecture

Figure 2.1 gives an overview of the proposed smart antenna. The architecture is fairly simple and it is composed of four antenna elements, and RF front-end circuit board, a digital control unit and a commercial IEEE 802.11b/g WLAN NIC (Network Interface Card).

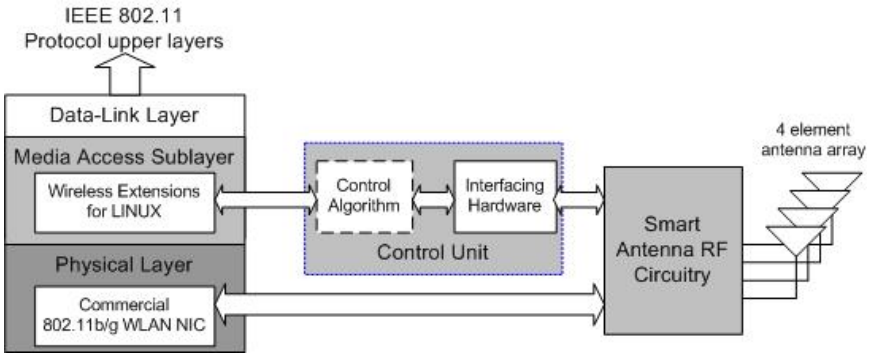

Figure 2.1: WLAN Smart Antenna System Block Diagram

2.2.1 Physical Layer

One of the main advantages of the system is its migration capability from one standard to another. Currently the system is used as an add-on external device to an existing NIC. The smart antenna is connected via an external antenna port through an SMA (Subminiature Version A) connector. This prototype was tested with an of-the-shelf WLAN USB (Universal Serial Bus) card.

2.2.2 Control Unit and MAC Layer

This first version of the smart antenna prototype system was implemented according to what is considered as the system's minimum configuration. Therefore the control system is based on the available parameter from the MAC (Media Access Control) sub-layer (the lower part of the Data Link layer), namely the RSSI of the system. The control system is able to work properly by using the RSSI signal to form a close loop system. The present control software exists over a LINUX based operation system that drives the RSSI from the NIC into a 128Kb microcontroller unit through the RS232 serial interface. This microcontroller will then apply control algorithms to control the prototype system.

2.2.3 RF Front-end

The RF frontend consists of three components: first stage RF frond-end board (antenna, band pass filter, and RF switch), LNA (Low Noise Amplifier)/PA (power Amplifier) combination and second stage RF front-end board (RF switch, second stage amplifier,

phase shifter network, and power combiner). The architecture presented can be defined as an Active RF Phase Shifter scheme. The idea is to have independent channels with independent RF components on each channel. The advantage is its expandability. Figure 2.2 shows the detailed block diagram of the RF frontend architecture.

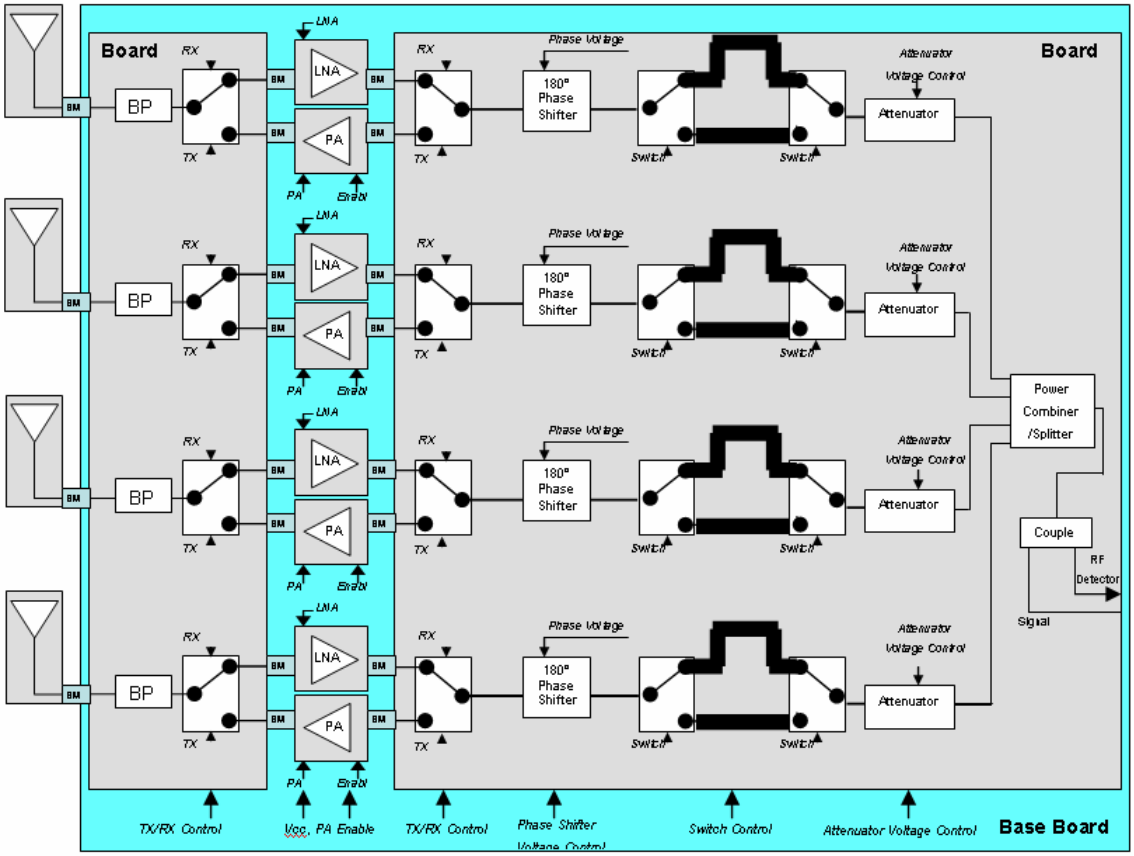

Figure 2.2: RF Front-end Block Diagram

2.3 RF Front-end Prototype and Components Testing Results

2.3.1 Antenna

In order to achieve the smart antenna capabilities at 802.11b/g frequency, we chose four antennas from TOKO Inc. with the part number of DAC2450CT1T. The TOKO DAC2450CT1T is a compact, vertically polarized, dielectric antenna specifically designed for 2.450 GHz applications including IEEE 802.11b/g wireless networking. The antenna unit consists of a dielectric element with a 50Ω termination resistance. This

permits us to directly connect the antenna to a 50Ω RF front end printed circuit board without designing a matching circuit. The miniature dimension allows the antenna to be attached to the prototype system easily. Table 2.1 illustrates the electronic and physical characteristics of the antenna.

Table 2.1: WLAN Antenna Characteristics

Miniature footprint	16 mm diameter
Low profile	6.5 mm
Center frequency	2450 MHz
Bandwidth	± 50 MHz
Peak gain	Less than +2.14 dBi (0 dBi typical)
Impedance	50Ω
Weight	4.3 grams

The four antennas are joined together in the same ground plane perpendicularly to the RF front end printed circuit board. The antenna ground place is 32cm (width) x 3cm (height) and it was designed over a FR4 printed circuit board with a thickness of 62 mils. In order to minimize coupling effect between adjacent antennas, the common design criteria is to space each two adjacent antennas with a distance of at least $\lambda/4$. Figure 2.3 shows a picture of the four antennas on the ground plane which is connected to the first stage RF front end board.

Figure 2.3: WLAN Antenna Layout with Ground Plan, BPF, and RF Switch

2.3.2 Band Pass Filter

An important requirement of the RF front end is band pass filtering. In receive mode the LNA should be protected from strong out of band signals to prevent blocking of the desired signal. In transmit mode, the spurious mixing products from the up converter

must be attenuated. Therefore, we chose a high frequency ceramic filter from Johanson Technologies with the part number 2450BP15B100. It has a maximum insertion loss of 2.2 dB and a reasonable out of band attenuation capability, about 10+ dB signal rejection. Table 2.2 shows the general specification of the band pass filter and Figure 2.4 shows S-parameter plots from 500MHz to 8GHz.

Table 2.2: BPF Characteristics

Frequency	2400MHz – 2500MHz	
Insertion loss	2.2dB Max	
Return loss	9.5dB Min	
Attenuation (min)	1200MHz – 1300MHz	25dB
Attenuation (min)	2000MHz	10dB
Attenuation (min)	3000MHz	12dB
Attenuation (min)	3600MHz – 3800MHz	30dB
Attenuation (min)	4800MHz – 5000MHz	34dB
Input power	500mW Max	
Impedance	50Ω	

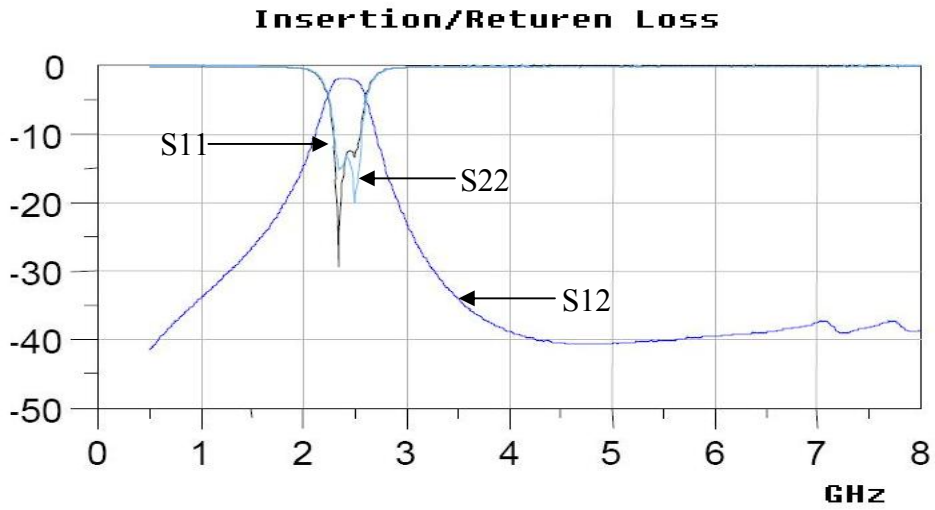

Figure 2.4: BPF S-Parameter Manufacture Testing Result

In our design, the BPF is located in the first stage RF frontend circuit board, between the antenna and RF switch. The following figure 2.5 shows the measured insertion loss of the BPF inside the PCB. The manufacture supplied data is marked with a cross signs. By observation, the insertion loss measured is extremely close to the manufacture supplied testing result.

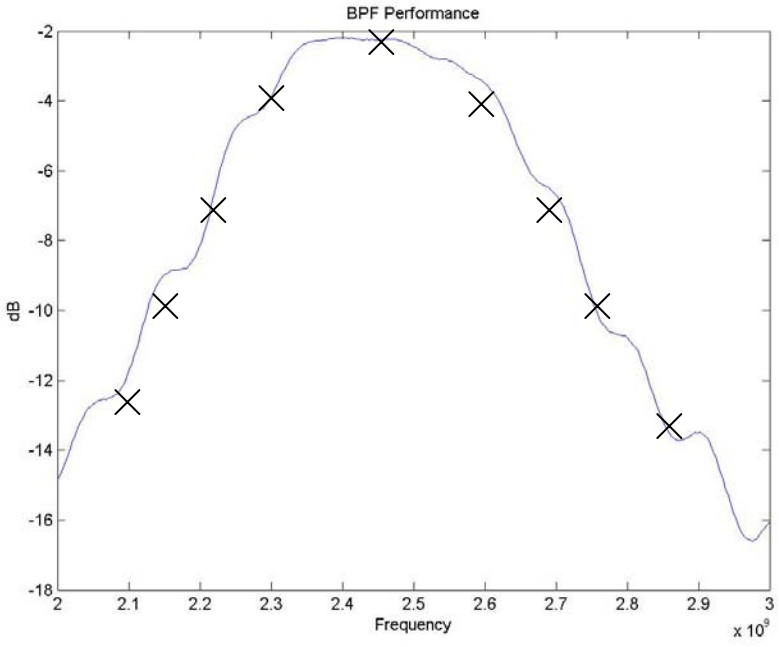

Figure 2.5: BPF Measured Insertion Loss

2.3.3 First Stage Low Noise Amplifier

The MAX2644, designed on a low-noise, advanced silicon-germanium (SiGe) technology, is an excellent choice for our WLAN application at 2.4GHz. While providing a 17dB gain with very low input third-order intercept point up to +4dBm, its noise figure is only about 1.8dB at 2.4GHz. It has on-chip output matching to 50Ω and uses a simple input matching topology for optimum noise figure.

The dynamic performance of the LNA is also very important. Since the LNA and PA form a half-duplex transceiving path, the LNA need to be shut off very quickly to allow PA to transmit. Any leakage from the LNA due to slow dynamic response will cause severe oscillation and saturate the channel, which in return saturate the processor in the

upper layer. Fortunately MAX2644 provides a fast time response suitable for our project. Since IEEE802.11b/g is a time-division duplexing (TDD) system, the LNA must have fast "Turn-ON and OFF" time in order to fulfill system requirement. Typically, 10ms is an acceptable limit. Lab measurement indicates that the Turn-ON time for the MAX2644 is approximately 8.6ms (power ramping up from less than -30dBm to -13dBm ±1dB). The Turn OFF time is 5ms for 30dB drop from nominal output power. Both timings meet the system requirement of 10ms. Table 2.3 shows the characteristics of MAX2644 LNA and please refer to Figure 2.6 for the gain and noise figure vs. frequency.

Table 2.3: LNA Characteristics

Operating frequency	2400MHz – 2500MHz
Gain	17dB
Input 1dB compression point	-13dBm
Noise figure	2dB
Input return loss	-15dB
Output return loss	-10dB
Reverse Isolation	-30dB

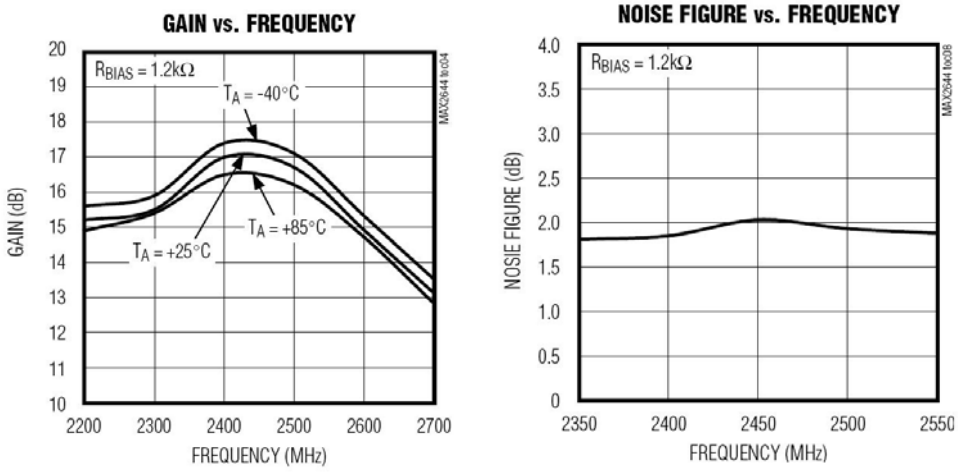

Figure 2.6: LNA Gain and NF Manufacture Testing Results

In order to make the design simpler, manufacturer's low noise amplifier evaluation boards (MAX2644EVKIT) were adapted to fit into the system. It was fully assembled and factory tested. The evaluation kit enables testing of the system performance more

easily and requires no additional support circuitry. It means that the input and output ports were pre-matched to 50Ω and were connected with SMA female connectors to facilitate easy connection of other RF equipment. Figure 2.7 shows the picture of the Maxim LNA evaluation kit.

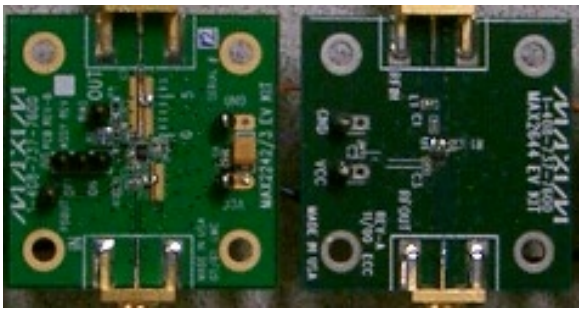

Figure 2.7: MAX LNA Evaluation Board

The following Figure 2.8 shows the measured S-parameter results of the Maxim LNA evaluation board using network analyzer.

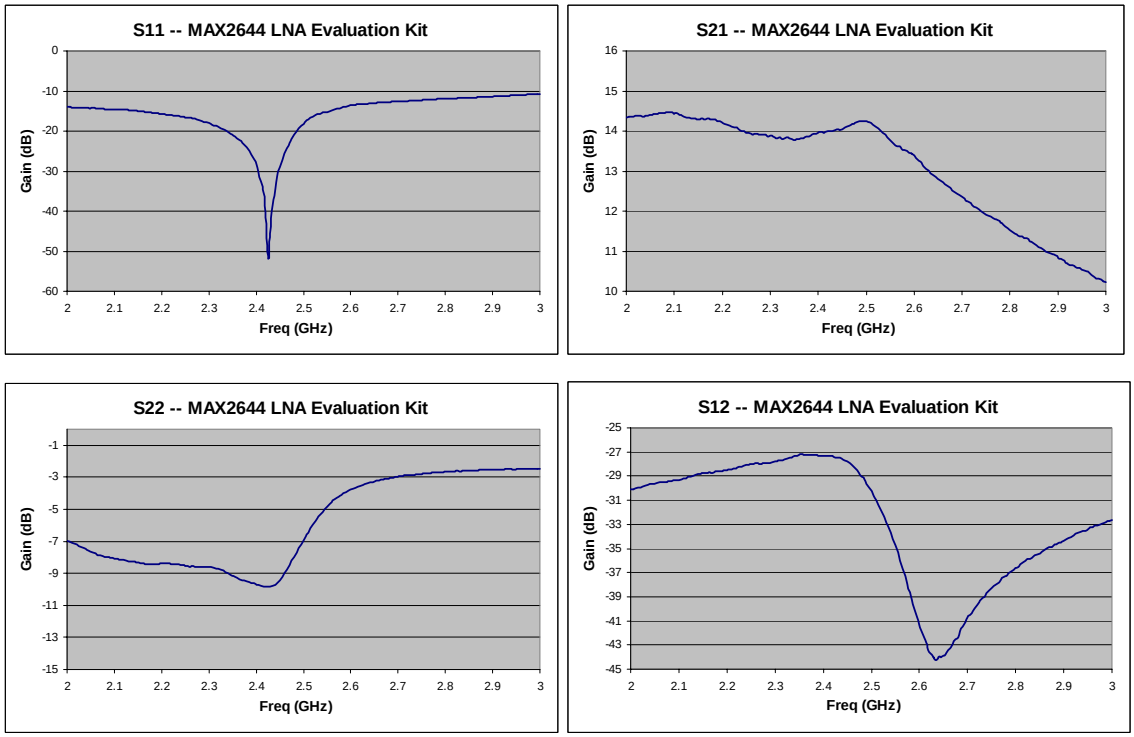

Figure 2.8: LNA S-Parameter Measured Results

From the S11 plot, it is noted that the LNA evaluation kit has a very good input matching circuit around 50Ω, about -20dB signal rejection between 2.4GHz to 2.5GHz.

S12 is very small which means there are very little signal that got reversed to the input port. S21 of the evaluation board is somewhat similar to the advertised gain of the MAX2644 chip except it is downgraded by about 2dB. This is partially caused by the loss from SMA connectors and the PCB. The design of the input/output matching circuit also contribute to the 2 dB gain reduction since the primary goal of the matching circuit is minimizing NF instead of maximizing gain. This is a very practical issue when designing supporting circuitry for LNA.

2.3.4 Second Stage Amplifier

In a cascaded system the overall NF is dominated by the characteristics of the first stage, since the effect of the second stage is reduced by the gain of the first, as illustrated in the following formula. NF_i is the NF of the i^{th} stage amplifier and G_i is the gain of the i^{th} stage amplifier.

$$NF_{overall} = NF_1 + \frac{1}{G_1}(NF_2 - 1) \tag{2.1}$$

Thus, for the best overall system noise performance, the first stage should have a low NF and at least moderate gain. Expense and effort should be devoted primarily to the first stage, as opposed to later stages, since later stages have a diminished impact on the overall NF [7].

Therefore in the two-stage amplification network, an inexpensive Gali-52 amplifier from Mini Circuits is used as the second stage amplifier. It has a typical gain of 17dB at 2.4GHz and a moderate NF of 2.7dB. Matching and bias network is designed for this amplifier. The following Table 2.4 illustrates the characteristic of Gali-52 amplifier.

Table 2.4: Gali-52 Amplifier Characteristics

Gain at 2GHz	17.8dB
Gain at 3GHz	15.9dB
Noise figure	2.7dB
Input 1dB compression point	32dBm

2.3.5 Power Amplifier

The transmit path is composed of MAX2242 power amplifier from Maxim. The MAX2242 low-voltage linear power amplifier works at 2.4GHz to 2.5GHz and delivers up to 22dBm of power output while consuming 1.6W of power. It provides a consistent 28.5dB of power gain across 2.4GHz to 2.5GHz, and across a wide range of input power. More importantly, it comes with an on-chip shutdown feature that reduces operating current to 0.5µA. This is a very important feature because of the half-duplex nature of WLAN operation. The control circuitry that will switch between the transmit path and receive path to ensure only one path is working at a time. Table 2.5 shows the characteristics of MAX2242.

Table 2.5: MAX2242 PA Characteristics

Frequency range	2400MHz – 2500MHz
Power gain	28.5dB
Output power	22.5dBm
Saturated output power, Pin = +5dBm	26.5dBm
Gain variation over Vcc +3V to +3.6V	±0.3dB

The following Figure 2.9 shows the output power vs. input power and it is observed that the PA has the best output amplification for input power less than -5dBm.

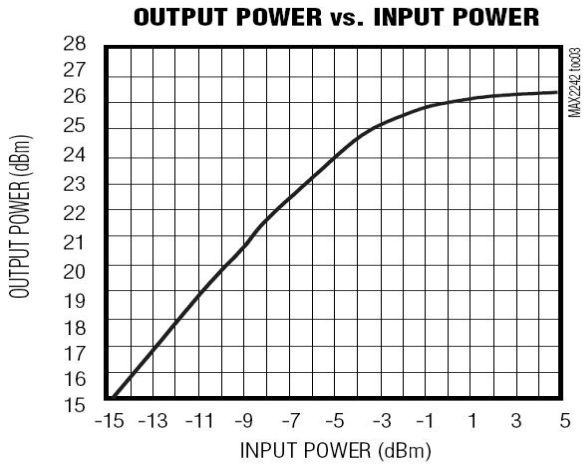

Figure 2.9: PA P_{in} vs. P_{out} Manufacture Testing Result

In order to make the design simpler, manufacturer's power amplifier evaluation boards (MAX2242EVKIT) were adapted to fit into the system. It was fully assembled and factory tested. The evaluation kit enables testing of the system performance more easily and requires no additional support circuitry. It means that the input and output ports were pre-matched to 50Ω and were connected with SMA female connectors to facilitate easy connection of other RF equipment. Figure 2.10 shows the picture of the Maxim power amplifier evaluation kit.

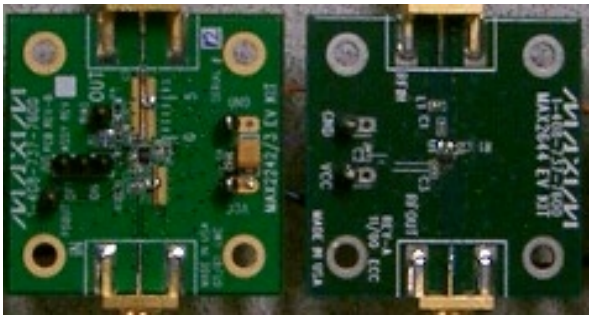

Figure 2.10: MAX PA Evaluation Board

The following Figure 2.11 shows the measured results of gain vs. frequency and output power vs. input power. They are very close to the advertised data.

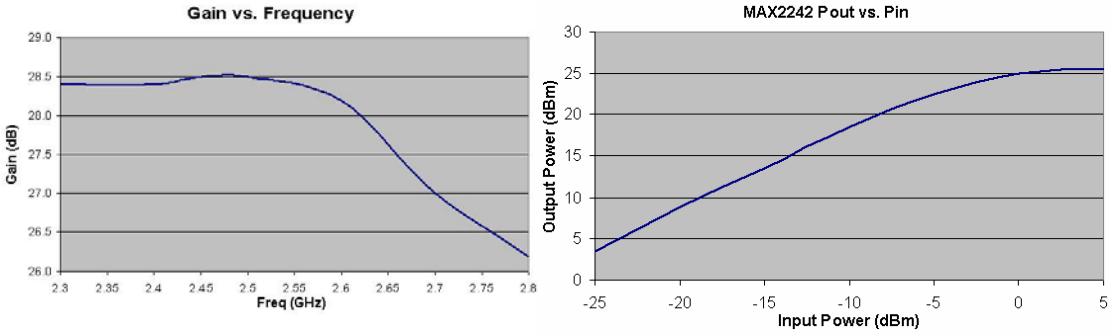

Figure 2.11: PA Gain and Power Measured Results

2.3.6 RF Switch

In this half-duplex transceiver design structure, the power amplifier and low noise amplifier must be connected to an antenna without adversely affecting the function of either device and with the minimum insertion loss added. The RF switch from Skyworks (AS169-73) is the ideal solution for solving this problem because it provides low

insertion loss (typically 0.4dB) and good isolation to the open contact port (typically 24dB). The fast switching time also made it perfect for the half-duplex switching control. Table 2.6 below shows the characteristics of the RF switch. Figure 2.12 and 2.13 shows the measured insertion and isolation results.

Table 2.6: Skyworks RF Switch Characteristics

Insertion loss at 2.4GHz	0.4dB typical
Isolation at 2.4GHz	24dB typical
VSWR at 2.4GHz	1.3:1 typical
Switching (rise/fall) time	10ns
Input power for 1dB compression at 2.4GHz	34dBm
IP3 at 2.4GHz	43dBm

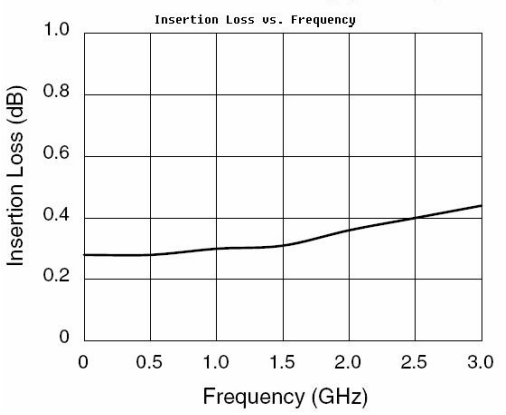

Figure 2.12: RF Switch Insertion Loss Measured Result

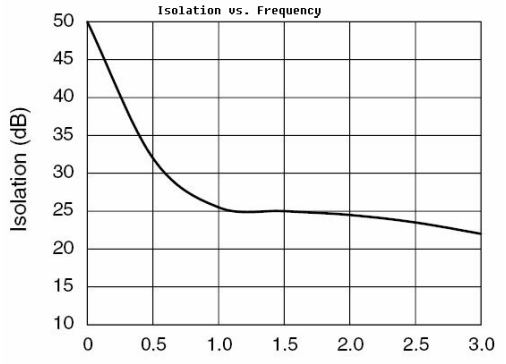

Figure 2.13: RF Switch Isolation Measured Result

2.3.7 Analog Phase shifters

The central part of the smart antenna architecture is the phase shifting capabilities of each channel. The history of practical analog beam forming antennas dates back to the Butler matrix [8], which consists of hybrid matrices and fixed phase shifters. Since the beam steering function is carried out by employing a selective RF switch, the steering angle is only discrete.

In our prototype design, the channel's ability to perform a continuous 0° to 360° phase shift during the adaptive beam scan enhances the RF signal gain dramatically. Due to the product availability and time constraint, we can only locate the 0° to 180° analog voltage controlled phase shifter chip. In order to carry out a 360° degree phase scan, another switch-controlled 180° transmission line is added to the design.

2.3.7.1 SVMicro 180° phase shifter

The only available off-the-shelf phase shifter IC is the surface mount voltage variable phase shifter from SV Microwave (part number VP242A-36C1) with a phase variation of about 180°. This phase shifter IC takes a variable voltage of 0 to 15 volt. It provides a low insertion loss up to 1.5dB and another great feature is its fairly linear phase response in its active voltage control region. Table 2.7 shows the characteristics of the phase shifter and Figure 2.14 shows the ideal phase shift vs. control voltage at 2.45GHz. Figure 2.15 shows the measured phase response in both transmit and receive mode.

Table 2.7: SVMicro Phase Shifter Characteristics

Insertion loss	1.1dB typical, 2dB max
Phase shift	200° typical, 180° min
Return loss	23dB typical
Control voltage	0 – 15V
Control current	20μA max

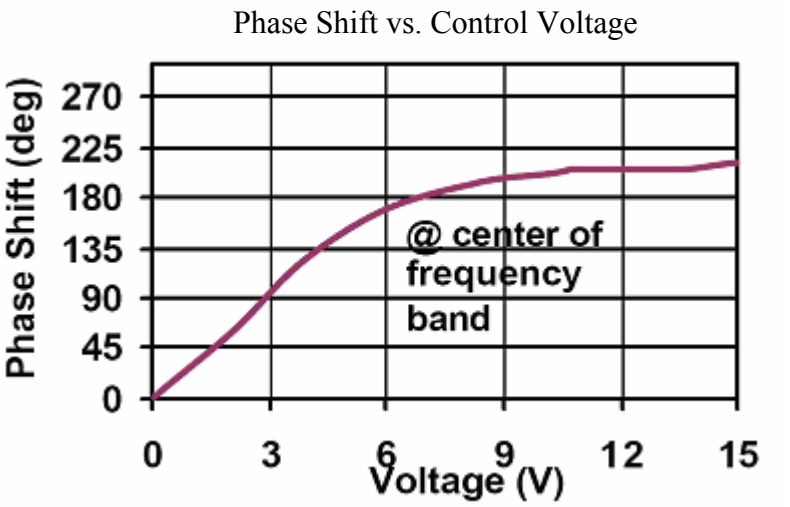

Figure 2.14: Phase Shifter Phase vs. Control Voltage Manufacture Testing Result

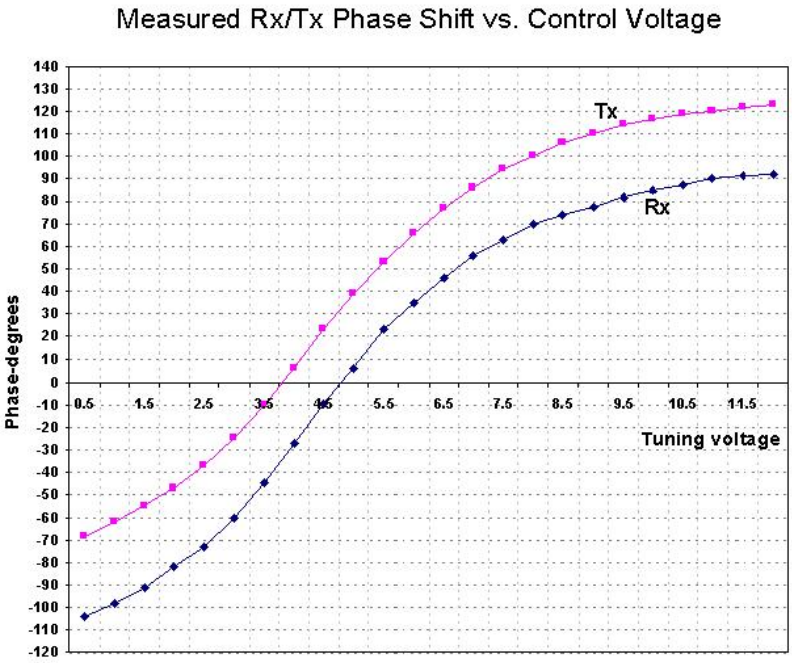

Figure 2.15: Phase Shifter Phase vs. Control Voltage Measured Result

It can be seen that the measured phase response is very close to the advertised response. The only disadvantage of the SVMicro phase shifter is its variable insertion

loss across voltage control because it most likely still uses a switch-based transmission line operation. An ideal variable phase shifter should have a constant loss/gain over the phase range, but a typical phase shifter like this one doesn't. Figure 2.16 shows the insertion loss variation vs. control voltages at 2.45GHz.

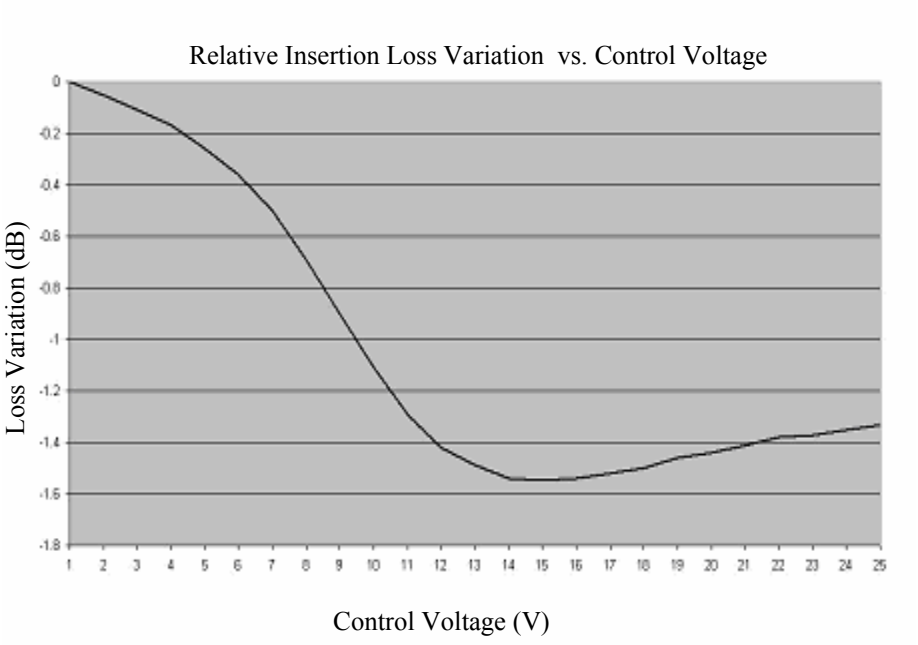

Figure 2.16: Variable Insertion Loss Measured Result

In smart antenna system this variable insertion loss can cause serious problems when we combine RF signals with different gains. This issue will be discussed and analyzed in the conclusion section of this chapter.

2.3.7.2 Design of 180° Microstrip Line Inverter

The designed microstrip line inverter consists of two RF microstrip line paths with a λ/2 length differences. A customized PCB is made to test the 180° microstrip line inverter as shown in Figure. It consists of one SMA connection and one RF switch on each side. Switching of the two paths is controlled by two RF switches. A 500μF capacitor is inserted in every segment of the transmission line to block DC voltage from passing through. A shutdown provision circuitry is included in the final system. The 180° phase

shifter designed and developed that changed the course of the research is shown in Figure 2.17.

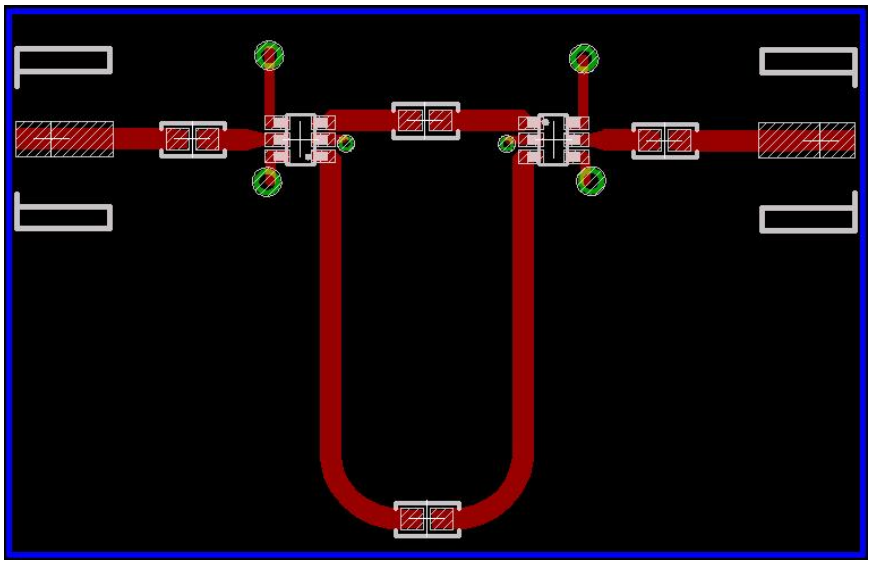

Figure 2.17: 180° Microstrip Line Inverter Layout

It is calculated with a microstrip line width (W) of 45mil, the characteristic impedance is 50.09Ω. The theoretical calculation is also verified by testing on fabricated prototype board with three different line widths. Figure 2.18 shows the S parameters of each individual testing.

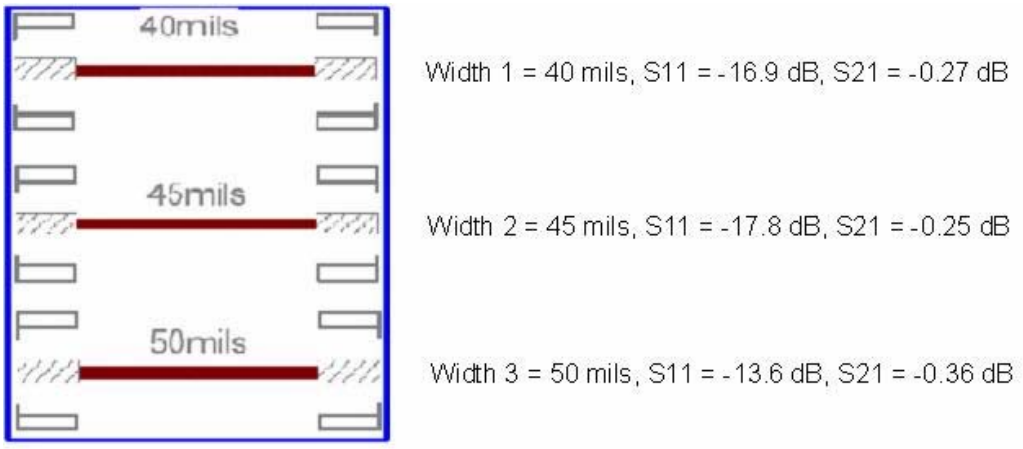

Figure 2.18: S-Parameter Measurements of Transmission Line

It is observed that the microstrip line of width 45mil gives the best S11 and S21 performances which also aligns with our theoretical calculation results.

2.3.8 Power Combiner

A four to one power combiner IC from MiniCircuits (part number SBD-4-25) is used for combining the receiving signals and splitting the transmitting signals. It provides around 20dB isolation and very good input and output port matching. Table 2.8 shows the characteristics of the power combiner IC at 2.45GHz.

Table 2.8: Power Combiner Characteristics

Isolation	22dB typical, 16dB min
Insertion loss	1dB typical, 1.8dB max
Phase unbalance	7° max
Amplitude unbalance	0.25dB typical, 07dB max
Input/output VSWR	1.26 typical

2.4 System Testing Results

As discussed in the previous section, the RF frontend of the prototype consists of three major components. They are again summarized in the following Table 2.9:

Table 2.9: WLAN RF Front-end Components Composition

RF Frontend Subsystem	**Components Included**
First stage RF frontend	Antennas, Band pass filters, RF switches
Amplification unit	LNA, PA
Second stage RF frontend	Amplifier, RF Switches, 360° Phase shifter network, channel shutdown provision circuitry, power combiner

The prototype system consists of four RF paths. The following figure shows the PCB layout of one RF path. Both receive path and transmit path were tested for each of the four channels. The receive path is divided into two stages of amplifiers. The first stage uses MAX2644 LNA which give about 15dB gain and 2dB noise figure. The second stage involves the use of GALI-52 amplifier from Mini-Circuits with gain of 17dB and noise figure of 2.7dB. PCB layout of a complete channel with both receive path and transmit path is illustrated in the following Figure 2.19.

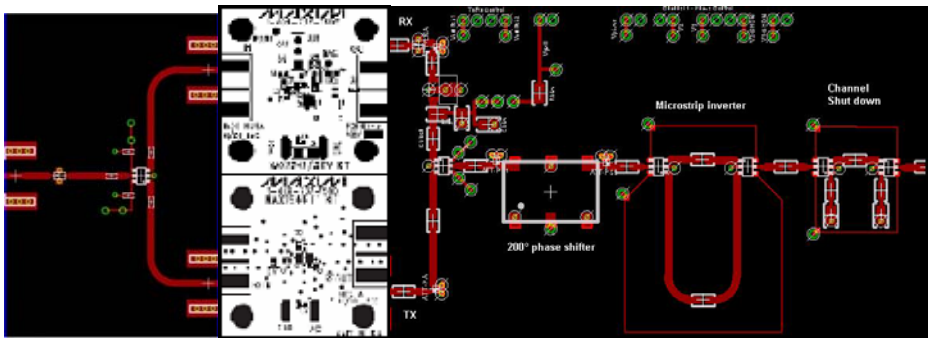

Figure 2.19: WLAN RF Front-end Single Channel PCB Layout

The complete receiving path, from BPF to the phase shifter network, gives about 12dB gain with less than 5.5dB of noise figure. The performance of four receive paths is shown in Figure 2.20. The antenna provides an average of 10-12dB gain for each of the four channels in the receive mode, and a relatively high return loss of -5dB. This is due to the imperfect of Maxim LNA evaluation board and the first stage and second stage RF front end PCB. The largest channel imbalance is about 2dB between channel one and channel three. The 2dB channel imbalance is contributed by the SVMicro phase shifter's variable insertion loss (about 1.6dB) across voltage control.

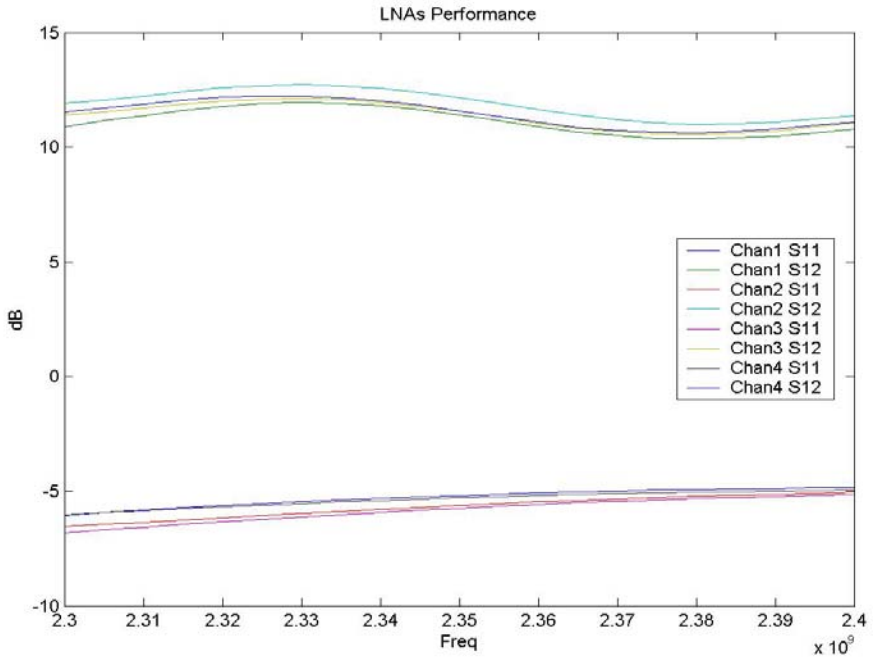

Figure 2.20: Receive Paths Measured Performance

The transmit path is only amplified by MAX2242 power amplifier and the performance of four transmit paths is shown in the following figure. The antenna provides an average of 11 dB gain for each of the four channels in transmit mode, and a return loss of -5dB. This large loss is due to the limitations on the components; namely, the Maxim PA evaluation board. The largest channel imbalance is about 0.5dB between channel one and channel three. Figure 2.21 shows the measured performance of transmit paths.

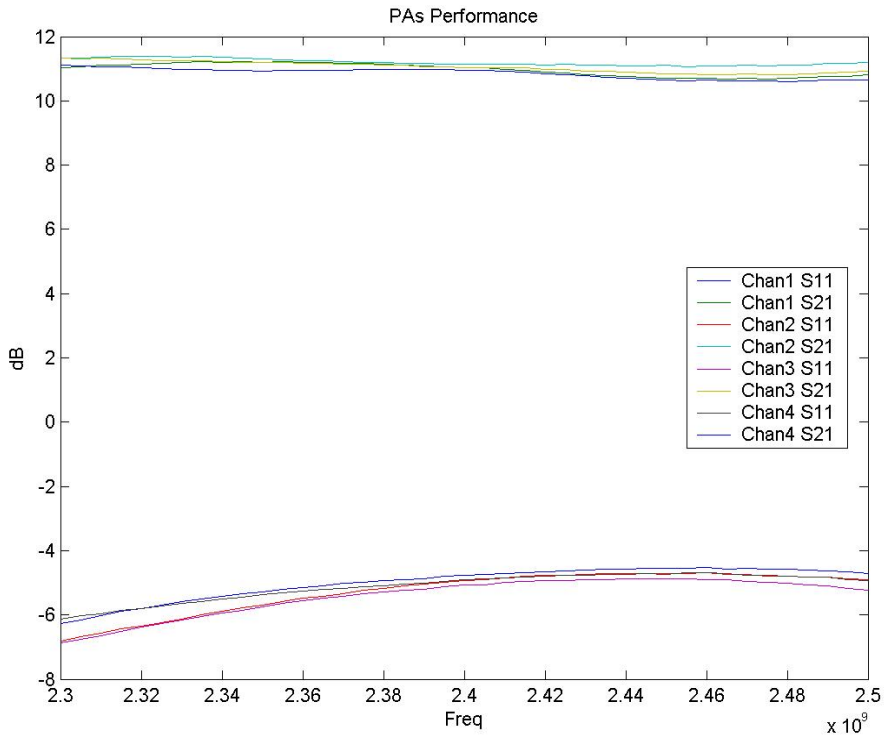

Figure 2.21: Transmit Paths Measured Performance

As it is shown previously, the receive path has a relatively large channel imbalance for about 2dB due to the variable insertion loss of the phase shifter. In fact, the variable insertion loss can cause serious problem in smart antenna system even though it has not been discussed thoroughly by previous researchers. Problem will arise when the signal gain by applying smart antenna technique is not sufficient enough to cover the additional phase shifter insertion loss when adjusting the control voltage as illustrated in Figure 2.22. This is particularly important for the smart antennas with very few low-gain elements.

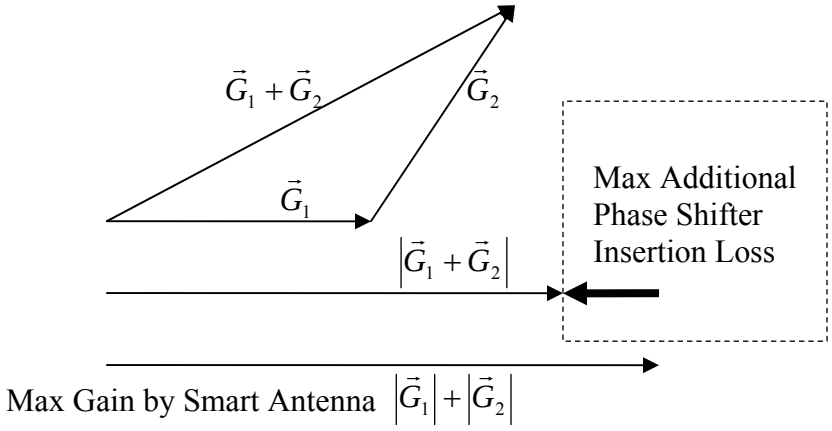

Figure 2.22: Maximum Additional Phase Shifter IL

From Figure 2.22, $\vec{G}_1$ and $\vec{G}_2$ are gains of two adjacent elements. The direct gain combination of the two elements with a magnitude of $\left|\vec{G}_1 + \vec{G}_2\right|$ is less than the optimized gain $\left|\vec{G}_1\right| + \left|\vec{G}_2\right|$ by using smart antenna to adjust the phase difference, only when the gain increase can overcome the phase shifter's insertion loss.

Let's work on two adjacent elements for example. Let the distance between the two adjacent antennas be 8cm and the elevation angle of the observation point be θ where θ is between 45° to 80°. The phase shift needed for maximum combined signal is:

$$\phi = 2N\pi - kd\cos\theta \text{ where } k = \omega\sqrt{\mu_0\varepsilon_0} \quad (2.6)$$

The following shows the matlab code to generate the extra gain by using smart antenna technique.

```
Function Variable_Insertion_Loss
d = 8e-2;
mu_0 = 1.2566e-6;
epsilon_0 = 8.8542e-12;
f = 2.4e+9;
k = 2*pi*f*sqrt(mu_0*epsilon_0);
for theta = 45:0.1:80
    phi = -k*d*cos(theta/180*pi)/pi*180;
    sum = sqrt(1+1-2*cos((180+phi)/180*pi));
```

```
    gain = 10*log10(2)-10*log10(sum);
    plot (theta, gain);
    hold on;
end
hold off;
```

Note that the maximum change of phase shifter's insertion loss is 1.6dB from Figure 2.16. Therefore the system might not be able to use smart antenna to steer the beam if the extra gain obtained is less than 1.6dB. This is illustrated in Figure 2.23. A threshold line is drawn in the plot indicating that the smart antenna system can not steer its beam effectively when the observation angle is over this value (66°), due to the phase shifter's variable insertion loss.

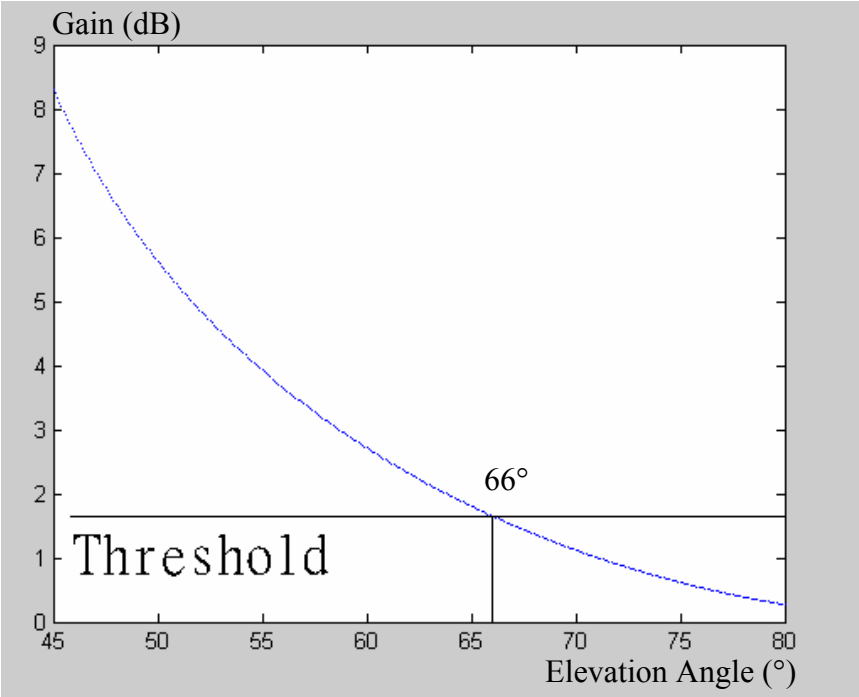

Figure 2.23: Elevation Angle Constraint

The combined RF signal from four channels is passed into a commercial WLAN NIC card for further signal processing such as signal mixing and down converting. The microcontroller then receives RSSI information from the NIC for beam control calculation purpose. The beam forming algorithm in the microcontroller relies on the

signal statistics gathered from an open-source Application Programming Interface (API) from the wireless extensions and tools from Linux, which lies above the MAC sublayer. The API provides signal statistics (RSSI) per network connection (MAC address per node), which can be used to experiment with tracking the relative position of other nodes. The obtained RSSI then is used to implement a proprietary adaptive algorithm that optimizes the received signal. The maximum RSSI delay given by the MAC sublayer is about 10ms. The algorithm takes approximately 720ms to adjust the antenna element pattern.

By controlling the phase shifters, initial testing results show a signal improvement of almost 25% in both the RSSI and SNR. Finally, the system's total power consumption is relatively small. There are 3 different supplies that are currently being used; 3.3V (for RF switches, LNA and PA), 5V (for microcontroller) and 10V (for second stage amplifier and phase shifter). Figure 2.24 shows the complete system which has the dimensions of 32x38x3.6cm.

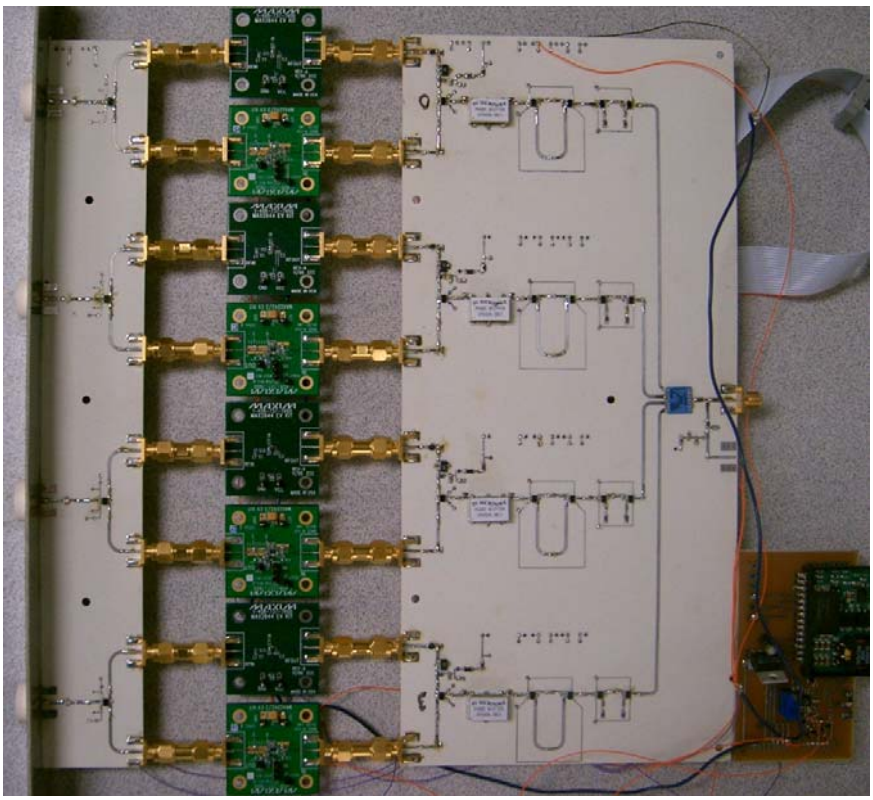

Figure 2.24: Complete WLAN RF Front-end

2.5 Conclusion

The system was successfully prototyped at 2.4GHz for the IEEE 802.11b/g WLAN protocol; its control mechanism is open, simple, and its implementation is extensible. We can put more advanced beam tracking algorithms such as LMS and SMI in the microprocessor to track the beam more accurately. We can also extend the system into eight channels or sixteen channels to increase the signal gain. On the other hand, the system's main limitation is its response time. Most of the latency is due to the retrieved RSSI time delay. Another limitation is its channel imbalances due to the phase shifter's variable insertion loss vs. control voltage.

Further development will allow the control algorithm to rely on the Physical Layer solely for getting the control parameters; thus, eliminating most of the latency. Also the current algorithm can only address a 4-element antenna array, but is not limited to it. The system is not portable but progress is being done for future development of a much simplified system with proprietary smart antenna RFIC chip transceivers, which include a variable 0° to 360° phase shifter with a constant insertion loss vs. control voltage. This will address the size and power consumption issues as well.

Chapter 3
Smart Antenna for SDARS Application

3.1 Introduction

Conventionally, consumer radio broadcasting service mainly consists of AM (Amplitude Modulation) radio broadcast and FM (Frequency Modulation) radio broadcast. AM radio can cover a very wide area but the reliability is low due to its vulnerability to interference and propagation variability. Its narrow band nature also limits the sound quality of its service. On the other hand, FM radio provides higher audio quality due to its higher operating frequency and therefore higher bandwidth. However, it covers less area than AM radio. It is therefore necessary to implement a third type of radio service that can not only cover a large area but also provide a high quality of audio service. SDARS (Satellite Digital Audio Radio Services) emerges as the perfect solution, as listeners are able to listen to the same list of CD-quality radio stations across the United States and Canada. Since 1991, two start-up companies, XM Radio and Sirius Radio have introduced this new type of radio broadcast which listeners are required to pay a low monthly fee. In fact, XM Radio has reached 6.5 million subscribers in April 2006 and Sirius Radio has reached 4 million by the end of March 2006.

The target SDARS users are consumers in mobile vehicles. The antenna used for reception can not be very expensive or the users will not be willing to purchase this service. So XM Radio and Sirius Radio are forced to abandon special high-gain antenna and complicated satellite tracking mechanisms used in other satellite communication services due to the high cost. In terms of antenna, the providers are forced to use omni directional antennas similar to the antennas used for mobile phones. Therefore, special diversity techniques such as ***spatial*** diversity, ***frequency*** diversity and ***time*** diversity are used to overcome reception problems of satellite communications [10]. In this paper, we will build a two-element antenna system. We will use smart antenna technique and

antenna diversity technique to overcome the multi-path reception problems and enhance the reception gain significantly by tracking the satellite signal.

3.2 Antenna Design and Simulation

3.2.1 Analysis and Design of a Single Microstrip Patch Antenna

Microstrip patch antennas are widely used in satellite communications, remote sensing, and military systems in the range of frequency from 1GHz up to 30GHz. Compatibility with planar technologies and the possibility of integrating microstrip elements with active circuits makes this type of antenna a unique candidate for cost-effective active integrated system and adaptive arrays wherein each antenna can be controlled individually. Such real-time spatial signal processing capability is becoming vital for many current and future applications. The following Figure 3.1 shows a top view and a cross view of a probe feed patch antenna.

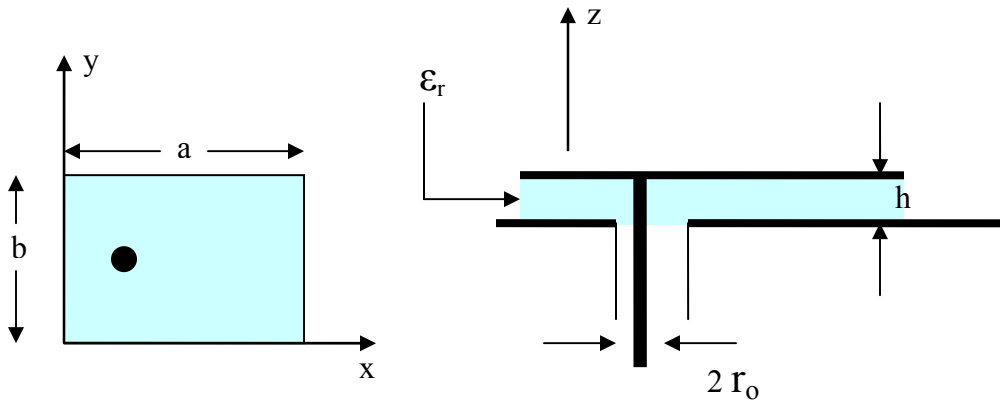

Figure 3.1: Microstrip Patch Antenna

Note that the patch antenna is basically an edge radiator. The radiated fields are generated by edge apertures namely two pairs of thin rectangular openings of dimension $a \times b$ and $b \times h$ respectively. To estimate the aperture fields the patch can be viewed as a thin rectangular resonant cavity of dimensions a, b, and h with the walls removed. The desired resonant mode is very similar to TM_{10} mode of a rectangular cavity. Therefore the dominant electric field component below the patch is:

$$E_Z = C_{10}\cos(\pi \cdot x/a) \tag{3.1}$$

The edge aperture fields generated by E_Z from equation 3.1 are:

$$\vec{E}_a \approx \hat{x}C_{10}\text{, along x = 0, a} \tag{3.2}$$

$$\vec{E}_a \approx \hat{y}C_{10}\cos(\pi \cdot x/a)\text{, along y = 0} \tag{3.3}$$

$$\vec{E}_a \approx -\hat{y}C_{10}\cos(\pi \cdot x/a)\text{, along y = b} \tag{3.4}$$

The far field radiation is given by:

$$\left|F(\psi,0)\right| = \left|\sin\psi\right|\left|\frac{\sin\left[k_0(b/2)\cos\psi\right]}{k_0(b/2)\cos\psi}\right|\text{, for H-Plane} \tag{3.5}$$

$$\left|F(\psi,90^0)\right| = \left|\cos\left(k_0\frac{a}{2}\sin\gamma\right)\right|\text{, for E-Plane} \tag{3.6}$$

Typically the substrate thickness, h, is less than a few hundredth of wavelength and length of the patch can be approximated as:

$$a \approx \frac{\lambda_d}{2} = \frac{\lambda_0}{2\sqrt{\varepsilon_r}}\text{, where } \varepsilon_r \text{ is the relative dielectric constant} \tag{3.7}$$

And the resonant frequency can be estimated as:

$$\omega_{10} = 2\pi \cdot f_{10} \approx \frac{2\pi \cdot c}{\lambda_0} = \frac{2\pi \cdot c}{\lambda_d\sqrt{\varepsilon_r}} = \frac{2\pi \cdot c}{2a\sqrt{\varepsilon_r}} = \frac{\pi}{a}\frac{1}{\sqrt{\mu_0\varepsilon_r\varepsilon_0}} \tag{3.8}$$

By applying the formulas above, a micro-strip patch antenna is designed at center frequency of 2.3GHz and laid out in Ansoft HFSS9 as it is shown in the following Figure 3.2. The metal patch has a dimension of 4cm × 5cm. Rogers 5880 substrate with a dielectric constant of 2.2 and thickness of 32mm has been used. A metal probe with a radius of 0.16cm has been created at a distance of 0.5cm from the center location on x-axis and an air box of 9cm × 10cm × 3.32cm is created around the antenna.

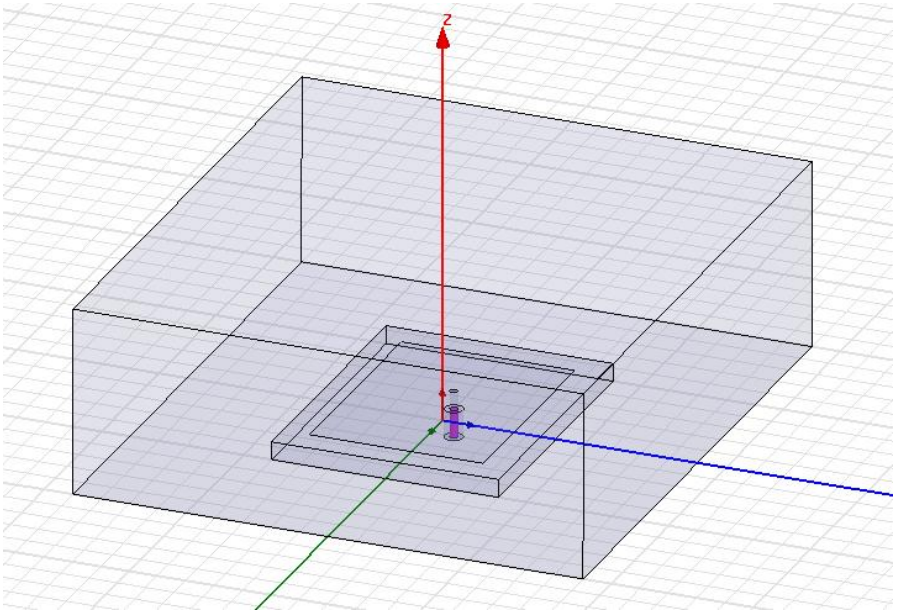

Figure 3.2: Single Patch Antenna Layout in HFSS

The location and dimension of the metal probe are found from previous experiment [11]. They provide a very good 50Ω port at the center frequency as shown in the following Figure 3.3. Within the center frequency between 2.3GHz to 2.4GHz, S11 is around -24dB.

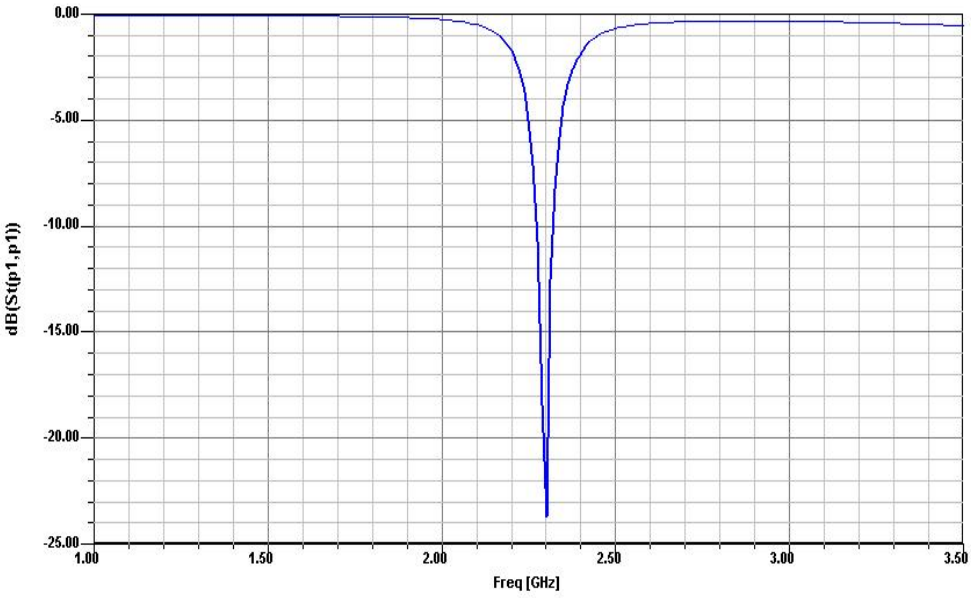

Figure 3.3: Simulated S11 of a Single Patch Antenna in HFSS

The far field radiation pattern is also simulated by using an air box with a dimension of 9cm × 10cm × 3.32cm. The radiation patterns at φ=0° and φ=90° are shown in the following Figure 3.4 with a maximum gain of 6.2dBi at the center direction.

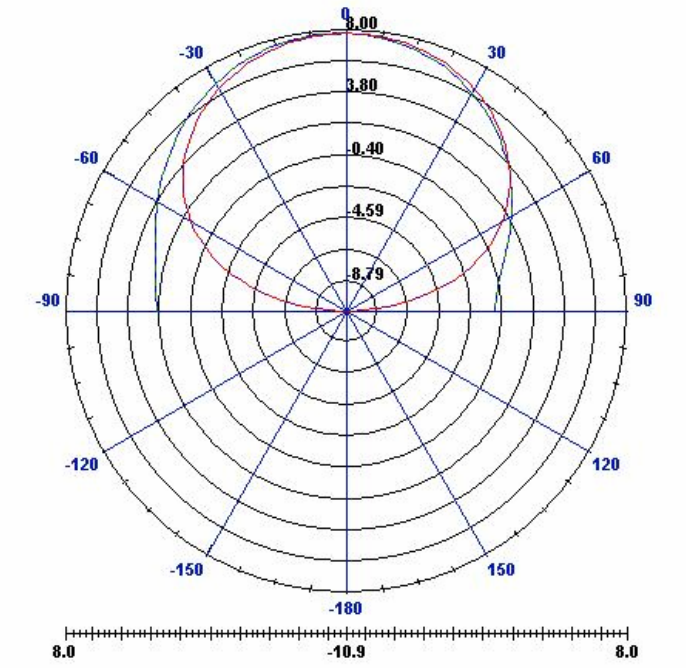

Figure 3.4: Far Field Radiation Pattern of a Single Patch Antenna

3.2.2 Two-Element Antenna System

Based on the successful design of a single micro-strip patch antenna at 2.3GHz, we locate two of such patch antennas on the adjacent side of a metal cubical box of dimension 5cm × 5cm × 5cm. A wave port is defined on the input surface of each metal probe. The configuration of the antenna elements has been chosen in order to maximize diversity gain and provide more than a hemispherical coverage (a wider reception angle). We intend to observe the far field radiation patterns of the combined signal by varying the phase difference between the two input feeds. The following Figure 3.5 shows the 3-dimensional layout of a two-element antenna system in HFSS.

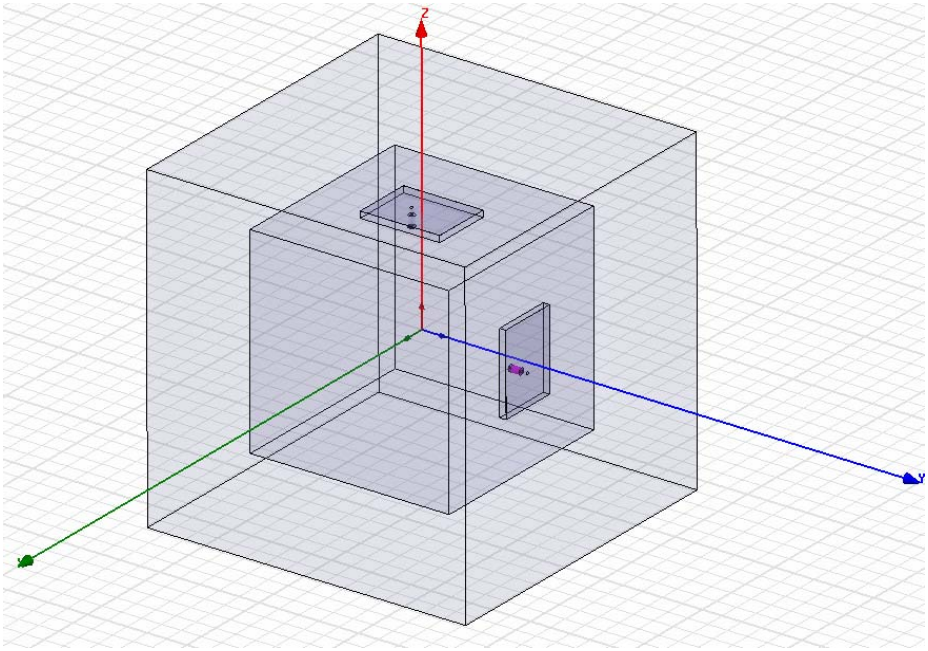

Figure 3.5: Conformal Antennas Layout in HFSS

By observing the combined far field radiation pattern from both sources, some very important observations can be found. In the first plot Figure 3.6, both sources have the same phase shifts, namely they are synchronized. In the second plot Figure 3.7, the two sources have 90° phase difference and in the last plot Figure 3.8 the two sources have 180° phase difference. It can be seen at elevation angle θ≈45°, the combined gain has a maximum of 5dB when two sources are added constructively. By contrast, the gain drops to -34dB when two sources are combined destructively.

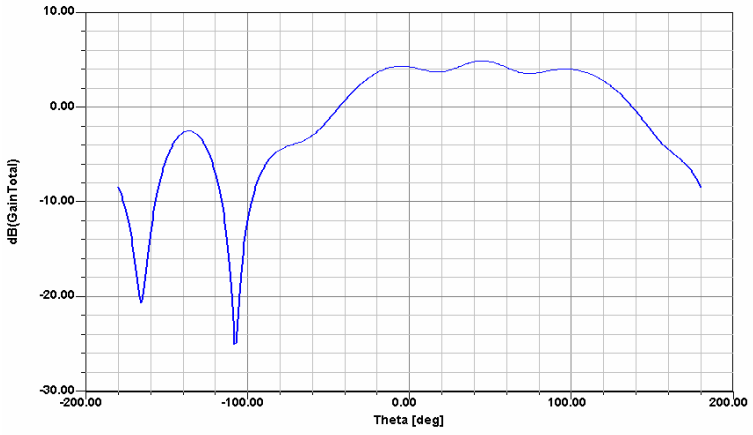

Figure 3.6: Radiation Pattern with 0° Phase Difference

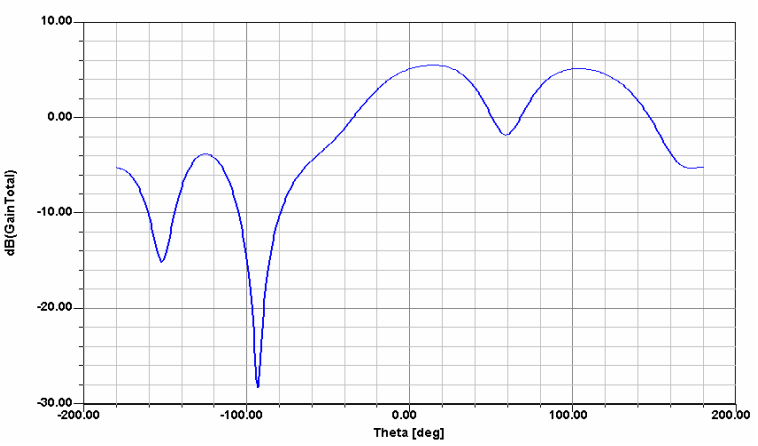

Figure 3.7: Radiation Pattern with 90° Phase Difference

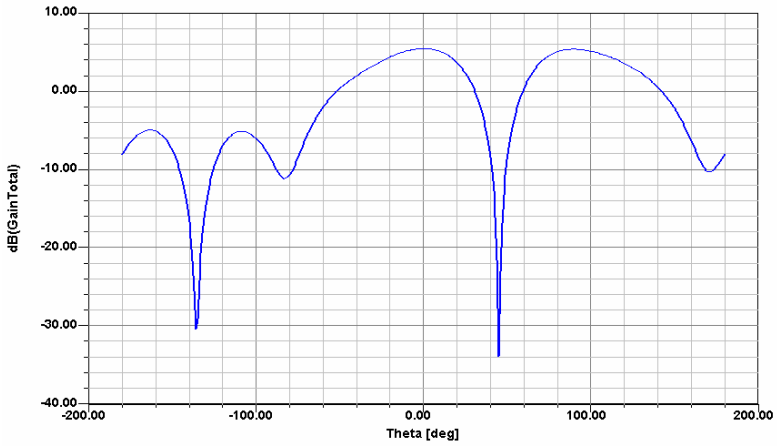

Figure 3.8: Radiation Pattern with 180° Phase Difference

Therefore, it is proven by simulation that when two antennas are combined together, the combined gain can be increased in most of the elevation angles. The covered area of two-element system is wider than a single element system (140° comparing to 90° for 3dB gain) if the phase differences between the two sources are adjusted correspondingly. In another word, the beam of the 2-element antenna system can be formed in certain desired direction by adjusting phases. Also, the huge signal decrease at 45° elevation angle suggests that the system is capable of performing interference nulling.

This two-element patch antenna system can be viewed as a two-port network with each port located at each antenna feed. The following Figure 3.9 shows the S11 and S12 of this

two-port network. It is interesting to find that at the distance between the maximum S12 and minimum S11 is at least 22dB, which indicate a very weak coupling effect between these two antennas. Therefore, it is valid to assume the radiation field caused by both antenna excitations is equal to the linear combination of the radiation field by each individual antenna. In fact, this assumption is tested and verified by simulation. From HFSS, we obtained far field radiation vectors from each antenna separately and we also obtained radiation vectors of the 2-element system. We found that the radiation vectors of the 2-element system are very close to the linear combination of the two single antennas radiation vectors. This finding can benefit future research on conformal antenna system and optimization method for EM wave calculation.

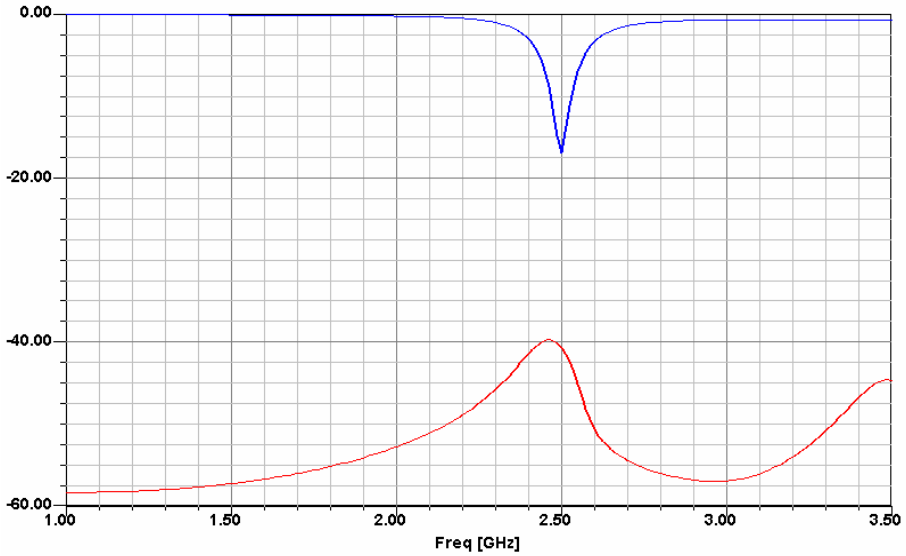

Figure 3.9: S11 and S12 of 2-element Antenna System

3.3 Smart Antenna RF Front-End Design for SDARS Application

The ability to receive CD quality satellite audio in a mobile vehicle places stringent requirements on the SDARS receiving antennas. The electrical requirements of SDARS antenna modules are outlined in the following Table 3.1.

Table 3.1: SDARS Antenna Requirements [9]

SDARS antenna-module performance		
PARAMETERS	SIRIUS	XM
Frequency band (MHz)	2320 to 2332.5	2332.5 to 2345
SAT antenna polarization	Left-hand circular	Left-hand circular
TER antenna polarization	Linear vertical	Linear vertical
SAT antenna gain (dBic)*	+2 to +4 (25 to 90 deg.)	+2 to +4 (20 to 60 deg.)
TER antenna gain (dBi)*	-1	-1
Current drain (mA)	150	90 to 110
Supply voltage (V)	5 to 8	4 to 5
SAT LNA gain (dB)	36	32
TER LNA gain (dB)	28	30
Max SAT LNA noise figure (dB)	0.7	0.7 to 1.2
Max TER LNA noise figure (dB)	2.0	1.5
Filter attenuation at ±250 MHz		25 to 35 dB

Note: The antenna was placed on the center of a 1-m-diameter ground plane.

Our objective is to design a two-element conformal antenna system for SDARS service that receives left hand circularly polarized satellite signal. Since automotive satellite receiver encounters multi-path effect and also signal attenuation, an inventive method is created to boost the reception signal level using smart antenna technique. Two antennas are placed on the adjacent surface of a metal box which can be viewed as a typical handheld receiver. Both antennas are connected to a LNA to increase the gain. One path is also connected to a 360° phase shifter. Finally two signal paths are jointed together using a 2-to-1 power combiner. The following Figure 3.10 shows the system block diagram.

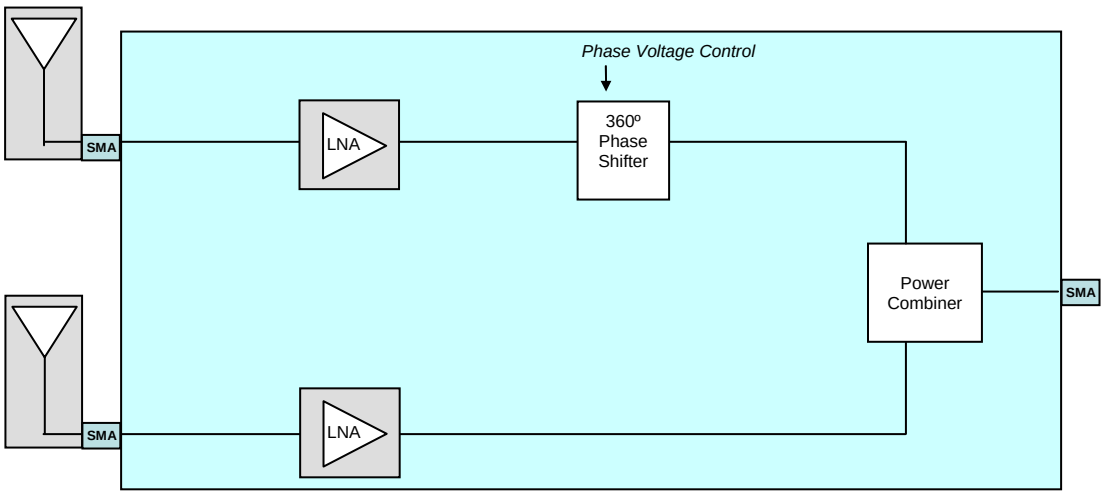

Figure 3.10: SDARS RF Front-end Block Diagram

3.3.1 Antenna

In order to achieve the smart antenna capabilities at 2.3GHz frequency for SDARS application, we chose two patch antennas from KYOCERA Inc. This standard SDARS patch antenna is compact, low profile and LHCP (Left Hand Circular Polarized). The antenna unit consists of ceramics dielectric material with a 50Ω termination resistance. This permits us to directly connect the antenna to a 50Ω RF front end printed circuit board without designing a matching circuit. The miniature dimension allows the antenna to be attached to the prototype system easily. Figure 3.11 shows the top view of the antenna and Table 3.2 illustrates the physical and electronic characteristics of the antenna measured on a 50mm × 50mm ground plane in free-space.

Figure 3.11: KYOCERA SDARS Antenna

Table 3.2: SDARS Antenna Characteristics

Size	$25mm^2 \times 4mm$ thickness
Frequency	2.3325GHz
Bandwidth	100MHz
Gain at Zenith	+5dBic
Impedance	50Ω
Polarization	LHCP

3.3.2 LNA

ZHL-1724HLN from MiniCiruits is selected as the LNA. It provides a high gain of 28dB with only 1.5-2dB NF. It takes 15V DC input power and it is packaged in a shielded metal box to avoid coupling and interference.

3.3.3 Phase Shifter

The same 180° phase shifter from SVMicro and a 180° switched transmission line from the WLAN system is used in the SDARS system to provide a continuous 360° phase shift.

3.4 Testing Results

Meanwhile, a two-element antenna box has been designed and tested to validate the theoretical simulation results. The box consists of two patch antennas (by KYOCERA) located on two adjacent side of a metal box. Inside the box, each probe of the antenna is connected to a LNA from MiniCircuits to boast the gain by 25dB.The box has a dimension of 9cm × 10.5cm × 22cm. The following is the picture of the antenna box.

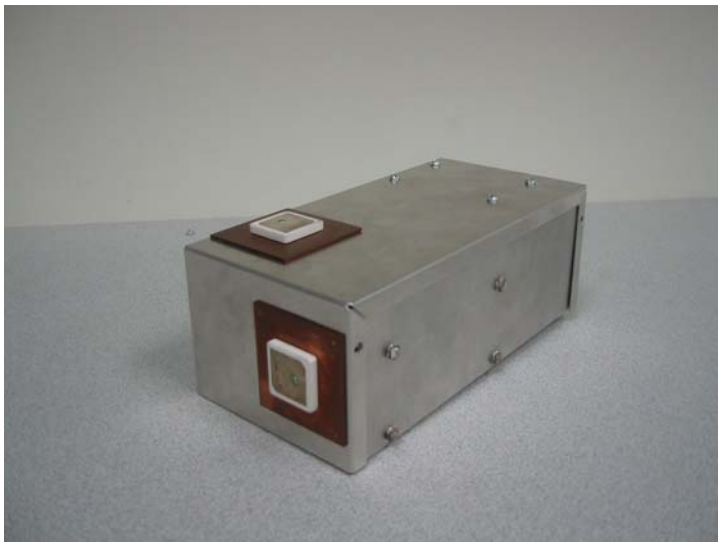

Figure 3.12: Actual SDARS Antenna Box

In order to perform a better test with less outdoor interference and multipath effect, we set up an indoor testing environment. It consists of the two-element antenna box with LNAs inside, a 360° phase shifter, a 2-to-1 power combiner, an RF signal generator and an RF spectrum analyzer. First of all, we connect a single wire antenna to an Agilent signal generator (E8267C PSG vector signal generator), which is set to output RF signal with center frequency of 2.332GHz and a bandwidth of 25MHz. This is to best simulate

the real SDARS frequency band. The following Figure 3.13 shows the signal generator with a wired antenna attached at the right bottom corner.

Figure 3.13: Signal Generator with Transmit Antenna

Then we hook up a spectrum analyzer (E4448A PSA spectrum analyzer from Agilent) to the output of the 2-to-1 power combiner. The spectrum analyzer is used to analyze the receiving signals as shown in the following Figure 3.14.

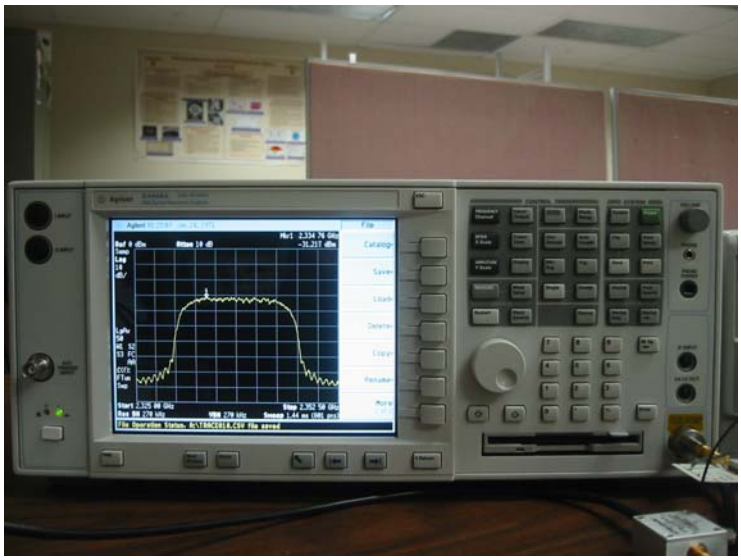

Figure 3.14: Spectrum Analyzer

The test is set up in such a way that both antennas have an equal distance and angle to the transmitter. This is done to provide equal gain to both antennas since smart antenna technique works the best when each individual channel has the same gain. For the proof of concept purpose, the receiver is located very close to the transmitter to eliminate signal refection. The setup block diagram is illustrated in the following Figure 3.15.

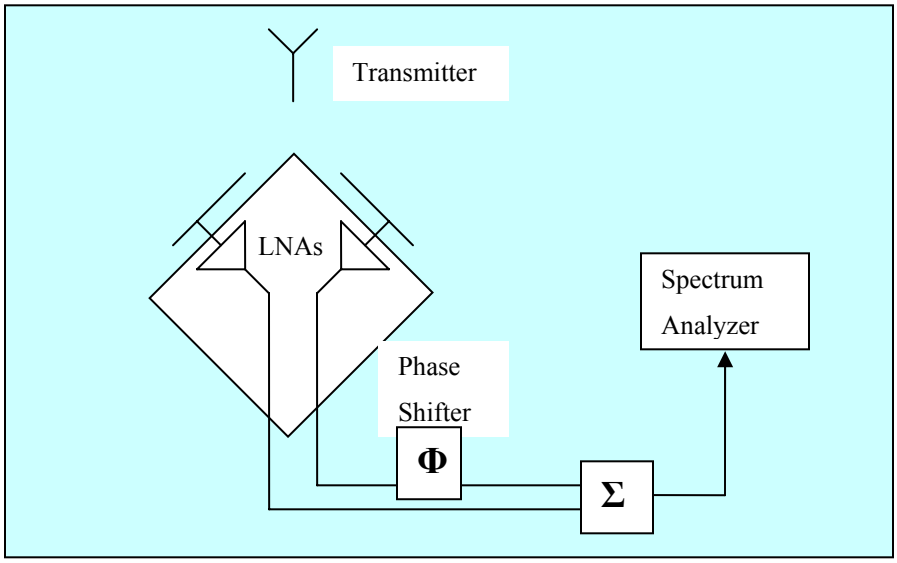

Figure 3.15: SDARS Test System Block Diagram

First of all, the receiving signals of both patch antennas are measured separately and plotted. Since they are located symmetrically, the frequency responses are very similar. Then two signals are combined with one path goes through a voltage controlled phase shifter. But varying the phase control voltage, a maximum and a minimum combined signal is obtained. This is illustrated inFigure 3.16. It is noted that the maximum combined gain is about 3-4 dB higher than each individual channel, and the weakest combined gain is about -40dB lower. The huge drop in the weak combined signal at 2.34GHz is occurred because the two channels are exactly out of phase at this frequency. The ideal scenario will be that the gain across the whole band is suppressed by -40dB. However, this is not very easy to realize because the phase difference is a function of frequency. Overall testing results match the results from simulation where the smart antenna technique can be used to increase the gain of the overall system across a wider receiving angle.

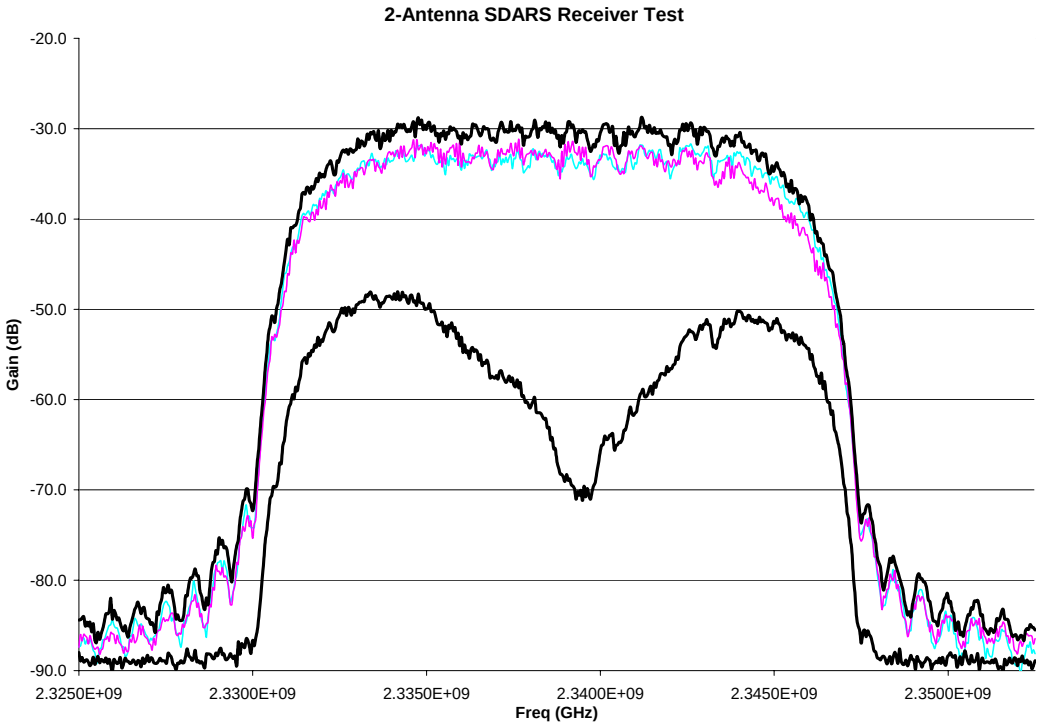

Figure 3.16: Spectrum Testing Results

The following Figure 3.17 is a screen shot of the weakest combined signal where the two input signals have a phase difference of 180° and are combined destructively.

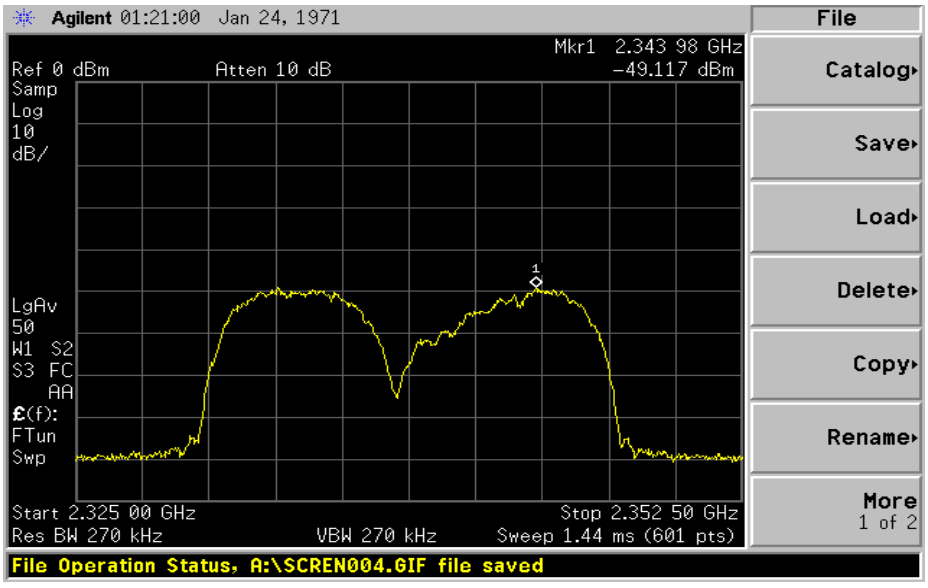

Figure 3.17: Weakest Combined Signal Screen Shot

As discussed in the introduction chapter, diversity mitigates severe multipath fading. Now it is also tested using the test setup shown in Figure 3.18. Because of multipath effect, by switching to stronger signal A, the output of the system is outperforming the combined signal also by at least 6 dB as illustrated from Figure 3.19. The top curve is the gain of antenna A and the bottom curve is the combined signal.

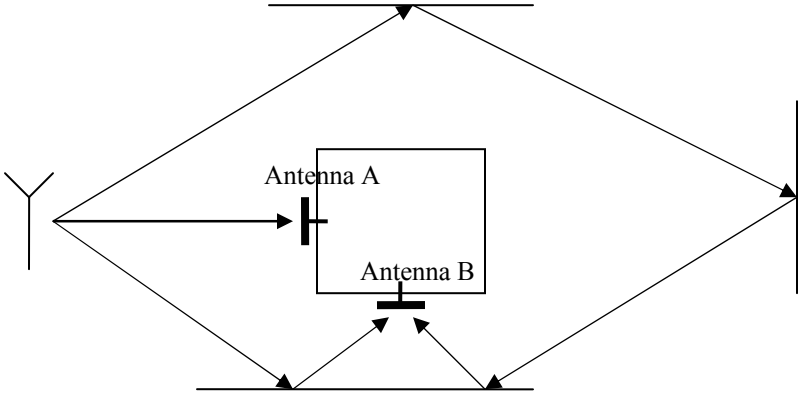

Figure 3.18: Diversity Test Setup

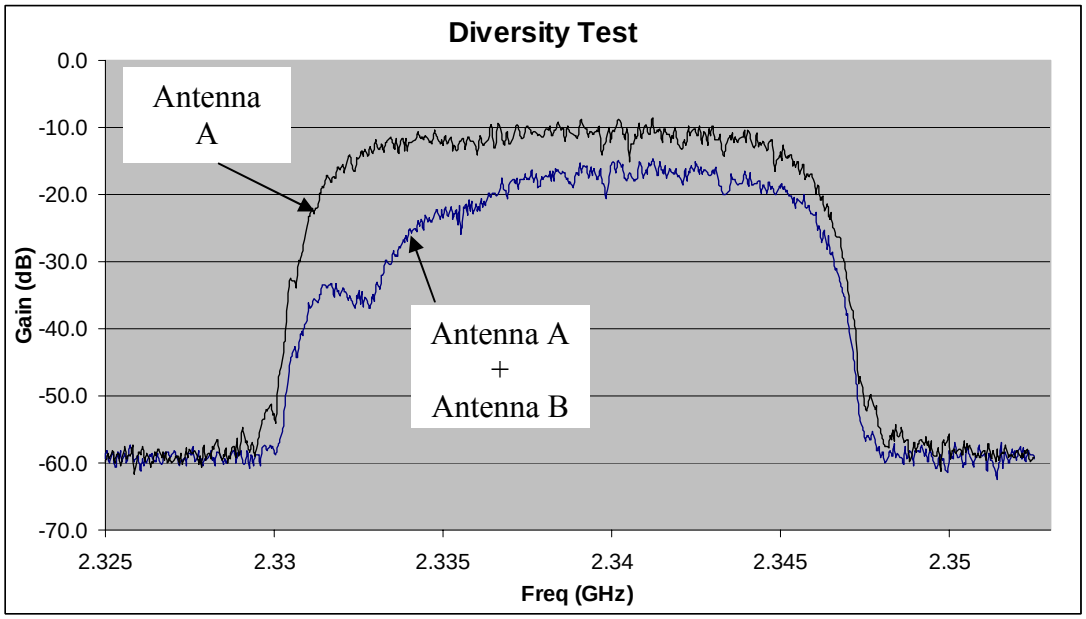

Figure 3.19: Diversity Test Result

Therefore with the full control of both amplitude and phase, we can have this 2-element smart antenna system work in any condition.

3.5 Conclusion

The two-element smart antenna system for SDARS is laid out and simulated in Ansoft HFSS. The simulation result shows that by introducing a phase difference between the two signal sources located on two adjacent side of a metal cube, the combined beam can be manipulated. In general, the total gain in certain direction increases when the two sources are combined constructively and the total gain drops dramatically when the two sources are combined destructively.

The simulation results from the two-element smart antenna system also unveil another interesting finding. It is known from antenna array system that the combined EM wave generated by the whole system is not equal to the sum of the EM wave generated by each individual antenna element because of the strong coupling effect between each antenna element. However in our experiment, simulation results show that the equality holds. This is due to the weak coupling between the two conformal antennas that are located on two adjacent perpendicularly located faces. This finding will benefit the future research on conformal antenna system and optimization method for EM wave calculation.

The system was successfully prototyped and tested in indoor environment and conditionally tested in outdoor environment. The test results show that:

- Coverage is widened by about 45° by using two-element antenna system.
- Maximum gain is increased by roughly 2dB by using smart antenna technique.
- Interference nulling can be realized by adjusting the phase difference to have signals combined destructively in the direction of interference. The gain in the central direction can be reduced from 5dB to -30dB.
- SNR is increased by about 2dB using diversity, reducing the negative effects of multipath signal fading.

Bibliography

[1] Kiran K. Shetty, "A novel algorithm for uplink interference suppression using smart antennas in mobile communications," Master of Science Thesis, Florida State University, Department of Electrical & Computer Engineering, 2004.

[2] Safieddin Safavi-Naeini, "Antenna and wireless systems," ECE476 course notes, University of Waterloo, Department of Electrical & Computer Engineering, pp. 40-42, 2004.

[3] International Engineering Consortium, "Smart antenna systems tutorial," pp. 2-4, 2005.

[4] Jack H. Winters, "Wireless technologies and information networks," World Technology Evaluation Center Inc., 2005.

[5] David R. Banbury, Nader Fayyaz, Safieddin Safavi-Naeini, and Sasan Nikneshan, "A CMOS 5.5/2.4 GHz dual-band smart antenna transceiver with a novel RF dual-band phase shifter for WLAN 802.11a/b/g," IEEE RFIC Symposium, pp. 157-160, June 2004.

[6] Seong-Sik Jeon, Yuanxun Wang, Yongxi Qian, and Tatsuo Itoh, "A novel planar array smart antenna system with hybrid analog-digital beamforming," 2001 IEEE MTT-S International Microwave Symposium, pp. 121-124, May 2001.

[7] David M. Pozar, "Microwave engineering," Second Edition, Wiley & Son Inc., pp. 558, 1998.

[8] Takashi Ohira, "Analog smart antennas: an overview," 2002 IEEE International Personal, Indoor and Mobile Radio Communications Symposium, Volume 3, pp. 1502-1506, 2002

[9] Argy Petros, and Imtiaz Zafar, "Antenna measurement techniques for SDARS antennas," Think Wireless Inc., 2002.

[10] David Bultman, "Satellite radio: the next communications revolution?," Internet article, http://engr.calvin.edu/PRibeiro_WEBPAGE/courses/engr302/Samples/Satellite%20Radio.doc

[11] “Design example – Probe Feed Patch Antenna, Ansoft high frequency structure simulator v9 user’s guide,” Ansoft Corp., 2004.